$\Delta S = 2$ and $\Delta C = 2$ bag parameters in the standard model and beyond from $N_f = 2 + 1 + 1$ twisted-mass lattice QCD

N. Carrasco,[1] P. Dimopoulos,[2,3] R. Frezzotti,[3,4] V. Lubicz,[1,5] G. C. Rossi,[2,3,4]
S. Simula,[1] and C. Tarantino[5,1]
(ETM Collaboration)

[1]*INFN, Sezione di Roma Tre Via della Vasca Navale 84, I-00146 Rome, Italy*
[2]*Centro Fermi—Museo Storico della Fisica e Centro Studi e Ricerche Enrico Fermi Compendio del Viminale, Piazza del Viminiale 1, I-00184 Rome, Italy*
[3]*Dipartimento di Fisica, Università di Roma "Tor Vergata" Via della Ricerca Scientifica 1, I-00133 Rome, Italy*
[4]*INFN, Sezione di "Tor Vergata" Via della Ricerca Scientifica 1, I-00133 Rome, Italy*
[5]*Dipartimento di Fisica, Università Roma Tre Via della Vasca Navale 84, I-00146 Rome, Italy*
(Received 5 June 2015; published 26 August 2015)

We present unquenched lattice QCD results for the matrix elements of four-fermion operators relevant to the description of the neutral K and D mixing in the standard model and its extensions. We have employed simulations with $N_f = 2 + 1 + 1$ dynamical sea quarks at three values of the lattice spacings in the interval 0.06–0.09 fm and pseudoscalar meson masses in the range 210–450 MeV. Our results are extrapolated to the continuum limit and to the physical pion mass. Renormalization constants have been determined nonperturbatively in the RI-MOM scheme. In particular, for the kaon bag parameter, which is relevant for the $\bar{K}^0 - K^0$ mixing in the standard model, we obtain $B_K^{\mathrm{RGI}} = 0.717(24)$.

DOI: 10.1103/PhysRevD.92.034516 PACS numbers: 12.38.Gc, 11.10.Gh, 11.15.Ha

I. INTRODUCTION

Lacking experimental data above production threshold, flavor physics offers the unique possibility for an indirect discovery of new physics (NP) effects through virtual exchanges of yet-to-be-discovered heavy particles in loop suppressed processes. This approach, which is particularly promising for processes that are highly suppressed within the standard model (SM), proved to be very successful in the past, allowing for the indirect determination of the charm and top quark mass [1–3].

Moreover, flavor physics data play a major role in providing stringent tests of the Cabibbo-Kobayashi-Maskawa (CKM) paradigm and allowing the determination of the magnitude of the mixing matrix elements. In particular, $\Delta S = 2$ and $\Delta B = 2$ flavor-changing neutral current processes are crucial to the unitarity triangle analysis. They are also quite valuable in constraining NP models; see, e.g., [4–11] with data on $\Delta S = 2$ oscillations providing the most stringent constraints [4–6,12].

Of special interest are the $\Delta C = 2$ transitions occurring in $\bar{D}^0 - D^0$ oscillations [13–15] and [16,17], as this is the only SM process in which mixing involves up-type quarks. CP violation through these mixings is expected to be strongly suppressed within the SM, because they are dominated by light (d, s) quark exchange, also entailing important long range interactions. Thus any experimental signal of CP violation in the neutral D meson sector would be a strong indication for the existence of NP [18–22]. Even in the absence of CP violation, our determination of $\Delta C = 2$ operator matrix elements allows to put constraints on models beyond the standard model (BSM).

In this paper we present a determination of the bag parameters relevant for the description of the $\Delta S = 2$ and $\Delta C = 2$ transitions. We compute meson-antimeson matrix elements of the whole basis of dimension-six four-fermion operators contributing the most general form of the effective $\Delta F = 2$ Hamiltonian [23–26]. Beyond the "left-left" operator, relevant for the SM, flavor-changing extra terms appear. The full effective $\Delta F = 2$ Hamiltonian reads

$$\mathcal{H}_{\mathrm{eff}}^{\Delta F=2} = \sum_{i=1}^{5} C_i(\mu)\hat{\mathcal{O}}_i(\mu) + \sum_{i=1}^{3} \tilde{C}_i(\mu)\hat{\tilde{\mathcal{O}}}_i(\mu), \qquad (1.1)$$

where C_i and $\tilde{C}_i$ are the Wilson coefficients and the bare operators, $\mathcal{O}_i$ and $\tilde{\mathcal{O}}_i$, corresponding to renormalized operators appearing in Eq. (1.1), are

$$\begin{aligned}
\mathcal{O}_1 &= [\bar{h}^\alpha\gamma_\mu(1-\gamma_5)\ell^\alpha][\bar{h}^\beta\gamma_\mu(1-\gamma_5)\ell^\beta], \qquad \tilde{\mathcal{O}}_1 = [\bar{h}^\alpha\gamma_\mu(1+\gamma_5)\ell^\alpha][\bar{h}^\beta\gamma_\mu(1+\gamma_5)\ell^\beta],\\
\mathcal{O}_2 &= [\bar{h}^\alpha(1-\gamma_5)\ell^\alpha][\bar{h}^\beta(1-\gamma_5)\ell^\beta], \qquad \tilde{\mathcal{O}}_2 = [\bar{h}^\alpha(1+\gamma_5)\ell^\alpha][\bar{h}^\beta(1+\gamma_5)\ell^\beta],\\
\mathcal{O}_3 &= [\bar{h}^\alpha(1-\gamma_5)\ell^\beta][\bar{h}^\beta(1-\gamma_5)\ell^\alpha], \qquad \tilde{\mathcal{O}}_3 = [\bar{h}^\alpha(1+\gamma_5)\ell^\beta][\bar{h}^\beta(1+\gamma_5)\ell^\alpha],\\
\mathcal{O}_4 &= [\bar{h}^\alpha(1-\gamma_5)\ell^\alpha][\bar{h}^\beta(1+\gamma_5)\ell^\beta],\\
\mathcal{O}_5 &= [\bar{h}^\alpha(1-\gamma_5)\ell^\beta][\bar{h}^\beta(1+\gamma_5)\ell^\alpha],
\end{aligned} \tag{1.2}$$

where α,β are color indices. The operators $\tilde{\mathcal{O}}_{1\text{–}3}$ are obtained from $\mathcal{O}_{1\text{–}3}$ with the replacement of $(1-\gamma_5)\to(1+\gamma_5)$. Since $\tilde{\mathcal{O}}_{1\text{–}3}$ and $\mathcal{O}_{1\text{–}3}$ have identical parity conserving parts, parity invariance of QCD allows to restrict our attention to only the set of operators $\mathcal{O}_i, i=1,\ldots,5$. In the present work we focus on the cases $(h,\ell)\equiv(s,d)$ and $(h,\ell)\equiv(c,u)$.

The Wilson coefficients describe short-distance effects. Accordingly, they will also depend on the heavy degrees of freedom possibly circulating in loops. The low-energy dynamics is incorporated in the matrix element of the operators $\hat{\mathcal{O}}_i$. The renormalization scale μ gets compensated between the Wilson coefficients and the matrix elements of the renormalized operators.

Lattice QCD provides a first principles determination of the bag parameters B_i. These are dimensionless quantities defined as the ratio of the nonperturbatively computed four-fermion matrix element over the value this matrix element takes in the vacuum saturation approximation. The reason for working with ratios is that they offer the advantage of a substantial cancellation of systematic and statistical uncertainties between the numerator and the denominator. Their definitions are (see, for example, Ref. [27])

$$\begin{aligned}
\langle\bar{P}^0|\mathcal{O}_1(\mu)|P^0\rangle &= \xi_1 B_1(\mu) m_{P^0}^2 f_{P^0}^2\\
\langle\bar{P}^0|\mathcal{O}_i(\mu)|P^0\rangle &= \xi_i B_i(\mu)\frac{m_{P^0}^4 f_{P^0}^2}{(m_\ell(\mu)+m_h(\mu))^2}\\
&\qquad \text{for } i=2,\ldots,5,
\end{aligned} \tag{1.3}$$

where $\xi_i=\{8/3,-5/3,1/3,2,2/3\}$ and P^0 stands for either a K^0 or a D^0 pseudoscalar meson. The corresponding mass and decay constant are denoted by[1] m_{P^0} and f_{P^0}, respectively. The quantities $m_\ell(\mu)$ and $m_h(\mu)$ are the light and heavy quark masses of the neutral K and D pseudoscalar mesons, renormalized at the scale μ.

We see from Eq. (1.3) that, while the matrix element $\langle\bar{P}^0|\mathcal{O}_1(\mu)|P^0\rangle$ vanishes as the pseudoscalar mass goes to zero, the four other matrix elements do not. We recall that B_1 parametrizes the SM operator while $B_i, i\geq 2$, parametrizes the BSM ones.

The computations presented in this paper have been performed making use of the $N_f=2+1+1$ dynamical quark gauge configurations generated by the European Twisted Mass Collaboration (ETMC) [28,29] at three values of the lattice spacing, $a\simeq 0.06$–0.09 fm, with the lightest pseudoscalar mass values in the range $M_{ps}\sim$ 210–450 MeV. Spatial lattice sizes are $L\simeq 2.1$–3.0 fm with $M_{ps}L\simeq 3.1$–4.5. Operator renormalization has been performed nonperturbatively in the regularization independent with momentum subtraction (RI-MOM) scheme [30].

A. Results

For the reader's convenience we immediately summarize our main results for K^0 and D^0 meson bag parameters.

We collect in Table I the values of the five bag parameters that are required to describe the neutral kaon mixing in the SM and beyond. We give the numbers in the $\overline{\text{MS}}$ renormalization scheme of Ref. [31] and in the RI′ scheme at the scale of $\mu=3$ GeV. For results given in the $\overline{\text{MS}}$ scheme the second quoted error provides our estimates for the systematic uncertainty coming from the perturbative matching between RI′ and $\overline{\text{MS}}$ schemes, which range from 0.5% to about 4%. The uncertainties on the central values stemming exclusively from our lattice computations are given by the first error and range from about 3.3% to 7.5%.

Neglecting the tiny over-unquenching error due to the presence of the charm in the sea (see discussion below) we adopt the continuum limit results in the $\overline{\text{MS}}$ scheme at $\mu=3$ GeV as our best estimate of the desired kaon mixing bag parameters in QCD with u, d and s active flavors for the same scheme and scale. Then for $B_K\equiv B_1$ we find in the renormalization group invariant (RGI) scheme the value[2]

$$B_K^{\text{RGI}(N_f=3)} = 0.717(24), \tag{1.4}$$

with a total uncertainty of about 3.4%.

In Table II we summarize the results for the bag parameters relevant for the case of the $\bar{D}^0-D^0$ oscillations.

[1]In our formulas we use the notation for a neutral pseudoscalar meson although we work in the isospin symmetric limit; so in practice we make no distinction between the masses and decay constants of the neutral and charged pseudoscalar mesons.

[2]If for converting our continuum limit B_1 in the $\overline{\text{MS}}$ scheme at $\mu=3$ GeV to its RGI counterpart we had taken $N_f=4$, we would have obtained $B_K^{\text{RGI}(N_f=4)}=0.728(24)$.

TABLE I. Continuum limit results for the bag parameters B_i $(i = 1, \ldots, 5)$ relevant to the $\bar{K}^0 - K^0$ mixing renormalized in the $\overline{\text{MS}}$ scheme of Ref. [31] and in the RI′ scheme at the scale of $\mu = 3$ GeV. For results given in the $\overline{\text{MS}}$ scheme the second error indicates an estimate for the systematic uncertainty owing to the perturbative matching of RI′ and $\overline{\text{MS}}$ schemes.

	$\bar{K}^0 - K^0$				
$\overline{\text{MS}}$ (3 GeV)	0.506(17)(3)	0.46(3)(1)	0.79(5)(1)	0.78(4)(3)	0.49(4)(1)
RI′ (3 GeV)	0.498(16)	0.62(3)	1.10(7)	0.98(5)	0.66(5)

TABLE II. Same as in Table I for the $\bar{D}^0 - D^0$ mixing.

	$\bar{D}^0 - D^0$				
$\overline{\text{MS}}$ (3 GeV)	0.757(27)(4)	0.65(3)(2)	0.96(8)(2)	0.91(5)(4)	0.97(7)(1)
RI′ (3 GeV)	0.744(27)	0.87(5)	1.34(11)	1.14(6)	1.39(9)

For results given in the $\overline{\text{MS}}$ scheme the second error we quote represents our estimate of the systematic uncertainty coming from the perturbative matching between RI′ and $\overline{\text{MS}}$ schemes. The uncertainties stemming only from our lattice computations are given by the first quoted error and range from about 4% to 8%.

The results of this paper are compared with the existing unquenched determinations[3] in Figs. 1, 2 and 3.

In Fig. 1 we present a compilation of recent (unquenched) RGI values of B_K. Lattice computations are quite accurate with a total uncertainty of only a few percent. It is worth noting the rather weak dependence of B_K^{RGI} on the number of dynamical flavors. Our current B_K^{RGI} value compares well with $N_f = 2 + 1$ and $N_f = 2$ lattice computations.

Our result is also found to be in agreement with the estimate obtained using a model based on the dual representation of QCD as a theory of weakly interacting mesons for large N, which predicts negative sign corrections to the large N limit estimate given by the value $B_K = 0.75$ [44,45].

A comparison of recent determinations of the $\bar{K}^0 - K^0$ bag parameters $B_i, i = 2, \ldots, 5$ is presented in Fig. 2.[4] The ETM, RBC/UKQCD and SWME collaborations give for B_2 and B_3 results that are well compatible within the errors. A tension of up to 3 standard deviations is visible, instead, in the case of B_4 and B_5 after the updated (preliminary) work of SWME [40].

Finally, in Fig. 3 we show the comparison of the available results for the D^0 bag parameters coming from ETMC computations with $N_f = 2$ and $N_f = 2 + 1 + 1$ gauge configurations.[5]

[3]For recent reviews, see Refs. [32,33].

[4]For older quenched computations of the BSM B_i, see Refs. [46,47].

[5]Work in progress of an unquenched $N_f = 2 + 1$ computation for the D-mixing is reported in Ref. [48]. For older works using quenched simulations, see Refs. [49,50].

Comparing the results for the bag parameters collected in Tables I and II with the ETMC results published in Refs. [12] and [43], the latter obtained with $N_f = 2$ dynamical quark simulations, we notice that they are all compatible among themselves and have similar total uncertainties. Therefore, *ceteris paribus*, the main conclusions presented in these works concerning model-independent constraints on the NP scale from $\Delta S = 2$ and $\Delta C = 2$ operators within the unitarity triangle analysis remain unchanged.

Before concluding this discussion, we find it useful to comment further about the dependence of B_K and of the other B-parameters for $\bar{K}^0 - K^0$ mixing on the number of dynamical quarks. As known, the standard theoretical formula that provides the indirect CP violation parameter ϵ_K is obtained, through the low-energy effective weak Hamiltonian, after integrating out the heavy degrees of freedom including the charm quark. The reason is that it is only when the charm quark is integrated out, i.e., at scales $\mu \sim m_c$, that the imaginary part of the effective Hamiltonian for $\bar{K}^0 - K^0$ mixing becomes local (at the leading order in the $1/m_c$ expansion). The advantage of this approach is that the long-distance contributions to the amplitude, being related to the matrix elements of local operators, are more easily accessible to lattice computations. The price to pay, however, is that perturbation theory is uncertain at scales around the charm mass and, in addition, subleading corrections proportional to powers of p_K^2/m_c^2 [where $p_K = \mathcal{O}(m_K, \Lambda_{\text{QCD}})$] may not be negligible, particularly when aiming at a theoretical prediction for ϵ_K with percent precision.

In the standard approach, both short-distance Wilson coefficient and long-distance matrix elements of the effective Hamiltonian have to be computed in the presence of three active quarks. In this respect, therefore, the lattice computation of B-parameters for $\bar{K}^0 - K^0$ mixing presented in this paper, being based on

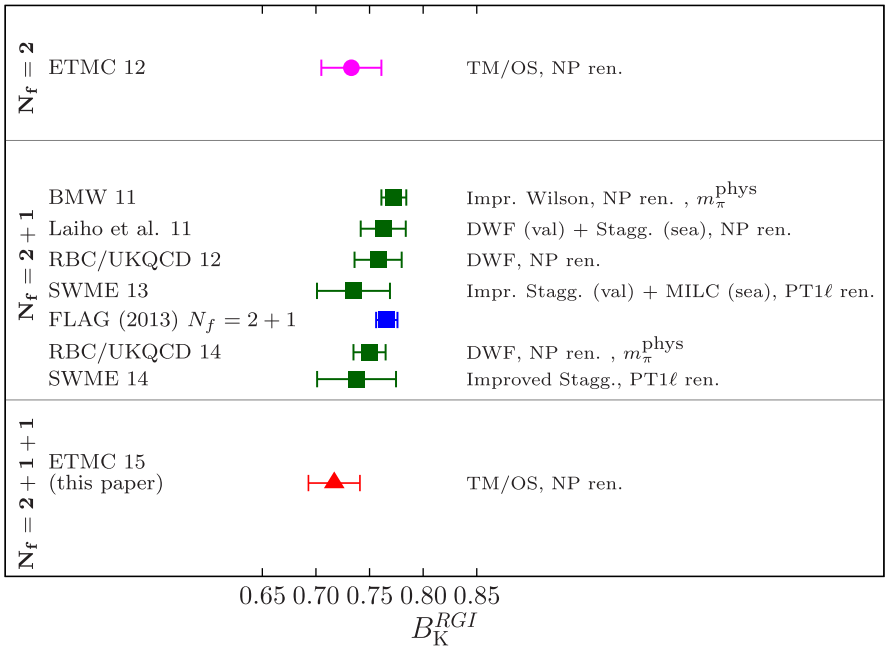

FIG. 1 (color online). A compilation of unquenched lattice results for the RGI value of the B_K parameter. From top to bottom results are taken from Refs. [12,32,34–39]. Circle, squares, and triangle correspond to $N_f = 2$, $N_f = 2+1$, and $N_f = 2+1+1$ dynamical quark computations, respectively. The full blue square indicates the FLAG average [32] over $N_f = 2+1$ data. For reader's convenience some information on the basic features of each computation is also given.

simulations performed with $N_f = 2+1+1$ dynamical quarks, introduces a systematic error. Previous experience with $N_f = 2+1+1$ lattice calculations suggests that the effect of the dynamical charm quark is presumably tiny, so that its impact in the determination of physical observables, which is undesired in this particular case, is likely too small to be detected at the level of the current precision.

It should be also noted that a similar source of systematic error is introduced in the lattice calculations of B_K performed with only $N_f = 2+1$ dynamical quarks. In the latter case, indeed, the effect of the dynamical charm, which properly is not introduced in the determination of the matrix elements, is missing however in the lattice computation of the hadronic observables which are needed to fix the action

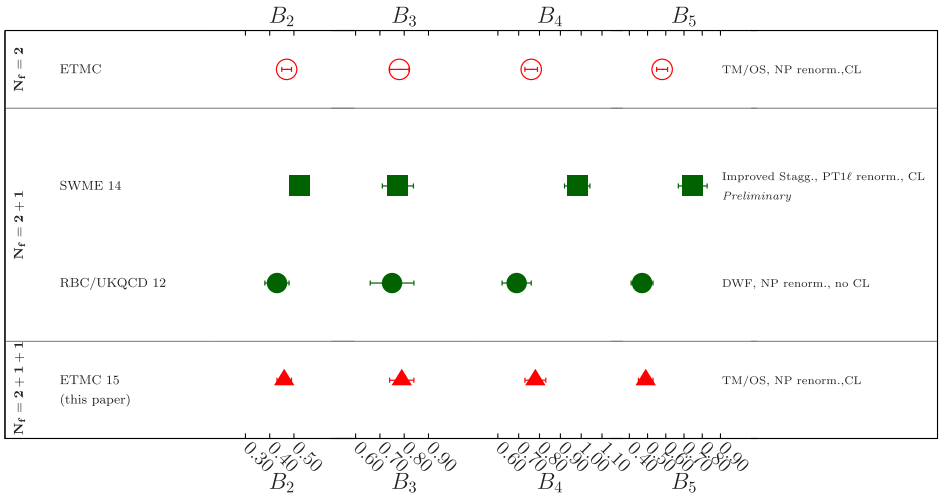

FIG. 2 (color online). A compilation of K^0 meson bag parameters B_i, $i = 2, \ldots, 5$. From top to bottom data have been taken from Refs. [12,40,41]. The work reported in Ref. [40] is an updated computation of Ref. [37]. The label "CL" stands for continuum limit computation. Work in progress by the RBC/UKQCD has been reported in [42].

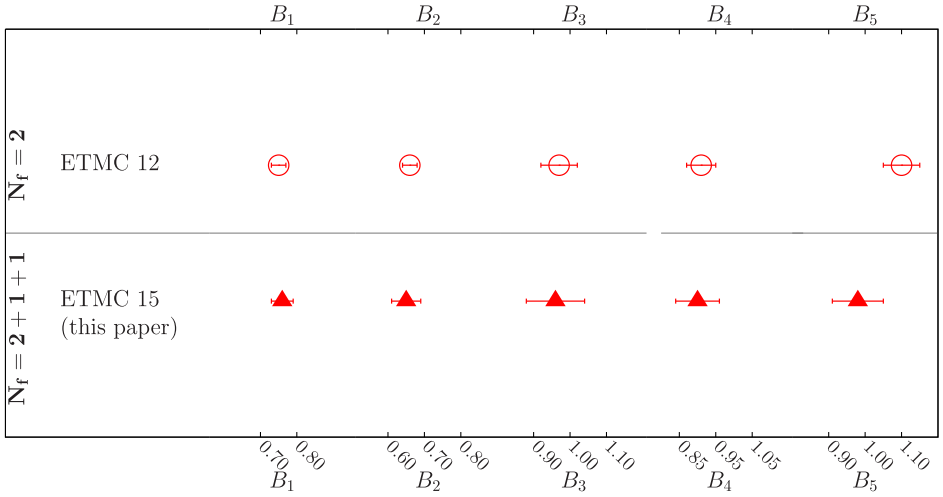

FIG. 3 (color online). Results for the D^0 meson bag parameters B_i, $i = 1, \ldots, 5$ obtained by the ETMC with $N_f = 2 + 1 + 1$ (this paper) and $N_f = 2$ [43] dynamical flavor lattice simulations.

parameters. Therefore, the determination of the lattice scale as well as of the strange and light quark masses within any $N_f = 2 + 1$ lattice calculation is affected by the systematic error due to the quenching of the charm quark. This error then propagates into the calculation of B_K. These effects, namely the latter one and the error introduced in the $N_f = 2 + 1 + 1$ calculations of B_K, have the same physical origin and are presumably comparable in size. As already noted, both effects are likely to be currently negligible, as also indicated, *a posteriori*, by the good consistency observed in Fig. 1 among the lattice determinations of B_K based on different numbers of active quarks.

In order to bypass this error, the theoretical determination of ϵ_K should be performed by keeping an active charm in the calculation. With the advances of the lattice technique, the computation of the matrix elements of nonlocal operators has becoming feasible and a first, exploratory lattice calculation of the real part of the effective Hamiltonian for $\bar{K}^0 - K^0$ mixing has been presented in Refs. [51,52]. The same technique can be also applied to the calculation of the imaginary part of the Hamiltonian, which is relevant for ϵ_K. While these lattice studies are not yet as accurate as the standard computations of local operator matrix elements, they are opening a new perspective and are likely to allow, in the near future, a significant improvement in the accuracy of the theoretical predictions of ϵ_K, for both the long-distance and short-distance contributions.

B. Plan of the paper

In Sec. II we review the simulation details and discuss our computational and analysis setup. Final results and a full account of the error budget are given in Sec. III. Finally, in the Appendixes A and B we discuss the procedure we employed to determine in RI-MOM the full 5×5 renormalization constants (RCs) matrix for the four-fermion operators.

II. COMPUTATIONAL DETAILS

In this work we have employed the mixed action twisted mass/Osterwalder-Seiler setup proposed in Ref. [53] which provides automatic $\mathcal{O}(a)$-improvement and a continuumlike renormalization pattern for the four-fermion operators, with only $O(a^2)$ unitarity violations.

A. Lattice setup

For the action of the light mass-degenerate sea quark doublet we have used the expression of Ref. [54] which reads

$$S_\ell = a^4 \sum_x \bar{\psi}_\ell(x) \left\{ \frac{1}{2}\gamma_\mu(\nabla_\mu + \nabla^*_\mu) - i\gamma_5\tau^3 \left[M_{\rm cr} - \frac{a}{2}\sum_\mu \nabla^*_\mu \nabla_\mu \right] + \mu_{\rm sea} \right\} \psi_\ell(x), \tag{2.1}$$

where it is intended that the untwisted mass has been tuned to its critical value, $M_{\rm cr}$. As usual, the symbols ∇_μ and ∇^*_μ represent the nearest neighbor forward and backward covariant derivatives, we define the quark doublet $\psi_\ell = (\psi_u \psi_d)^T$, and $\mu_{\rm sea}$ is the (light) sea twisted quark mass.

With similar notations we take the action for the strange and charm quark doublet in the sea [55] to be

$$S_h = a^4 \sum_x \bar{\psi}_h(x) \left\{ \frac{1}{2}\gamma_\mu(\nabla_\mu + \nabla^*_\mu) - i\gamma_5\tau^1 \left[M_{\rm cr} - \frac{a}{2}\sum_\mu \nabla^*_\mu \nabla_\mu \right] + \mu_\sigma + \mu_\delta \tau^3 \right\} \psi_h(x), \tag{2.2}$$

where μ_σ and μ_δ are the bare twisted-mass parameters from which the renormalized strange and charm masses can be derived. Pauli matrices in Eqs. (2.1) and (2.2) act in flavor space. For more details on the twisted-mass setup see Refs. [28,29,54–58].

Valence quarks are introduced via Osterwalder-Seiler (OS) fermions [59]. The valence action is written as the sum of the *individual* quark flavor contributions in the form

$$S^{\rm OS} = a^4 \sum_x \sum_{f=\ell,\ell',h,h'} \bar{q}_f \left\{ \frac{1}{2}\gamma_\mu(\nabla_\mu + \nabla^*_\mu) - i\gamma_5 r_f \left[M_{\rm cr} - \frac{a}{2}\sum_\mu \nabla^*_\mu \nabla_\mu \right] + \mu_f \right\} q_f(x), \tag{2.3}$$

where the label f is allowed to run over the different valence flavors $f = \ell, \ell', h, h'$. In the neutral K case light (ℓ) and heavy (h) flavors denote down and strange quarks, respectively, while in the neutral D-case they stand for up and charm quarks. With the choice $r_h = r_\ell = r_{h'} = -r_{\ell'}$ one can prove [53] that at maximal twist automatic $\mathrm{O}(a)$ improvement and absence of wrong chiral mixings [60] is guaranteed. Flavor by flavor bare valence and sea quark masses are set equal to each other which is enough to keep unitarity violations to $\mathrm{O}(a^2)$. The multiplicative mass renormalization constant is Z_P for all fermions.

The lattice setup described above has been already successfully applied to determine the full set of four-fermion operator matrix elements relevant for the $\bar{K}^0 - K^0$, $\bar{D}^0 - D^0$ and $\bar{B}^0_{(s)} - B^0_{(s)}$ oscillations in Refs. [12,43,61–63].

B. Simulation details

We have used $N_f = 2 + 1 + 1$ gauge configuration ensembles, produced with the Iwasaki gluon action [64] and maximally twisted Wilson fermions, generated by the ETM Collaboration [28,29].

In Table III we summarize the main simulation details relevant for the sea and valence sector. Simulation data have been taken at three values of the lattice spacing, namely, $a = 0.0885(36)$, $0.0815(30)$, and $0.0619(18)$ fm, corresponding to $\beta = 1.90$, 1.95, and 2.10, respectively (see Ref. [65]).

As we said, light valence and sea quark masses are set equal, leading to pion masses in the range between 210 and 450 MeV. Strange and charm sea quark masses are chosen close to their physical value. To allow for a smooth interpolation to the physical values of the strange and charm quark mass, we have inverted the heavy valence Dirac matrix for three values, $\mu_{\text{“}s\text{”}}$, of the strange quark mass and three values, $\mu_{\text{“}c\text{”}}$, of the charm mass, around the corresponding physical mass values.

The lattice scale has been fixed using f_π. The u/d, strange, and charm quark masses have been determined by comparing them with the experimental values of the pion,

TABLE III. Details of the simulation setup. Sea and valence fermion actions are displayed in Eqs. (2.1), (2.2), and (2.3).

β	$L^3 \times T$	$a\mu_\ell = a\mu_{\rm sea}$		$a\mu_{\text{“}s\text{”}}$			$a\mu_{\text{“}c\text{”}}$	
1.90 ($a^{-1} \sim 2.19$ GeV)	$24^3 \times 48$	0.0040	0.0145	0.0185	0.0225	0.21256	0.25	0.29404
$\mu_\sigma = 0.15$ $\mu_\delta = 0.19$		0.0060						
		0.0080						
		0.0100						
	$32^3 \times 64$	0.0030	0.0145	0.0185	0.0225	0.21256	0.25	0.29404
		0.0040						
		0.0050						
1.95 ($a^{-1} \sim 2.50$ GeV)	$24^3 \times 48$	0.0085	0.0141	0.0180	0.0219	0.18705	0.22	0.25875
$\mu_\sigma = 0.135$ $\mu_\delta = 0.17$	$32^3 \times 64$	0.0025	0.0141	0.0180	0.0219	0.18705	0.22	0.25875
		0.0035						
		0.0055						
		0.0075						
2.10 ($a^{-1} \sim 3.23$ GeV)	$48^3 \times 96$	0.0015	0.0118	0.0151	0.0184	0.14454	0.17	0.19995
$\mu_\sigma = 0.12$ $\mu_\delta = 0.1385$		0.0020						
		0.0030						

K, and $D_{(s)}$ meson masses, respectively. Further details of our simulation setup can be found in Ref. [65].

Valence light and strange quark propagators have been computed by employing spatial stochastic sources at a randomly chosen time slice, adopting the "one-end" trick stochastic method of Refs. [66,67]. In correlators where the charm quark is involved, Gaussian smeared interpolating quark fields [68] are used in order to suppress the contribution of excited states. This allows ground state identification at precocious Euclidean time separations.

For the values of the smearing parameters we take the $k_G = 4$ and $N_G = 30$ Gaussian. In addition, we apply APE smearing to the gauge links [69] in the interpolating fields with parameters $\alpha_{\rm APE} = 0.5$ and $N_{\rm APE} = 20$.

C. Lattice operators and bag parameters

A detailed account of the lattice operators entering two- and three-point correlation functions was presented in Appendix A of Ref. [62]. For the reader's convenience and to fix the notation we recall here some basic information. In our mixed action setup one needs to consider the following set of four-fermion operators:

$$
\begin{aligned}
O^{\rm MA}_{1[\pm]} &= 2\{([\bar{q}^\alpha_h\gamma_\mu q^\alpha_\ell][\bar{q}^\beta_{h'}\gamma_\mu q^\beta_{\ell'}] + [\bar{q}^\alpha_h\gamma_\mu\gamma_5 q^\alpha_\ell][\bar{q}^\beta_{h'}\gamma_\mu\gamma_5 q^\beta_{\ell'}]) \pm (\ell \leftrightarrow \ell')\}\\
O^{\rm MA}_{2[\pm]} &= 2\{([\bar{q}^\alpha_h q^\alpha_\ell][\bar{q}^\beta_{h'} q^\beta_{\ell'}] + [\bar{q}^\alpha_h\gamma_5 q^\alpha_\ell][\bar{q}^\beta_{h'}\gamma_5 q^\beta_{\ell'}]) \pm (\ell \leftrightarrow \ell')\}\\
O^{\rm MA}_{3[\pm]} &= 2\{([\bar{q}^\alpha_h q^\beta_\ell][\bar{q}^\beta_{h'} q^\alpha_{\ell'}] + [\bar{q}^\alpha_h\gamma_5 q^\beta_\ell][\bar{q}^\beta_{h'}\gamma_5 q^\alpha_{\ell'}]) \pm (\ell \leftrightarrow \ell')\}\\
O^{\rm MA}_{4[\pm]} &= 2\{([\bar{q}^\alpha_h q^\alpha_\ell][\bar{q}^\beta_{h'} q^\beta_{\ell'}] - [\bar{q}^\alpha_h\gamma_5 q^\alpha_\ell][\bar{q}^\beta_{h'}\gamma_5 q^\beta_{\ell'}]) \pm (\ell \leftrightarrow \ell')\}\\
O^{\rm MA}_{5[\pm]} &= 2\{([\bar{q}^\alpha_h q^\beta_\ell][\bar{q}^\beta_{h'} q^\alpha_{\ell'}] - [\bar{q}^\alpha_h\gamma_5 q^\beta_\ell][\bar{q}^\beta_{h'}\gamma_5 q^\alpha_{\ell'}]) \pm (\ell \leftrightarrow \ell')\},
\end{aligned}
\tag{2.4}
$$

where α and β are color indices, the square parentheses denote spin covariant operator factors and the label "MA" stands for "mixed action."

We have set periodic boundary conditions for all fields, except for the quark fields which obey antiperiodic boundary conditions in the time direction. Two "wall" operators with P^0-meson quantum numbers (recall P^0 can be either K^0 or D^0) are introduced at time slices y_0 and $y_0 + T_{\rm sep}/2$. The first operator is constructed in terms of q_ℓ and q_h quark fields and the second in terms of $q_{\ell'}$ and q'_h quark fields. Explicitly they are given by

$$
\begin{aligned}
\mathcal{P}^{\ell h}_{y_0} &= \left(\frac{a}{L}\right)^3 \sum_{\vec{y}} \bar{q}_\ell(\vec{y}, y_0)\gamma_5 q_h(\vec{y}, y_0)\\
\mathcal{P}^{\ell' h'}_{y_0+T_{\rm sep}} &= \left(\frac{a}{L}\right)^3 \sum_{\vec{y}} \bar{q}_{\ell'}(\vec{y}, y_0 + T_{\rm sep})\gamma_5 q_{h'}(\vec{y}, y_0 + T_{\rm sep}).
\end{aligned}
\tag{2.5}
$$

In terms of them, the correlation functions we need to calculate are

$$
C_i(x_0) = \left(\frac{a}{L}\right)^3 \sum_{\vec{x}} \langle \mathcal{P}^{\ell' h'}_{y_0+T_{\rm sep}} O^{\rm MA}_{i[+]}(\vec{x}, x_0)\mathcal{P}^{\ell h}_{y_0}\rangle, \quad i = 1, \ldots, 5, \tag{2.6}
$$

$$
C_{XP}(x_0) = \left(\frac{a}{L}\right)^3 \sum_{\vec{x}} \langle X^{h\ell}(\vec{x}, x_0)\mathcal{P}^{\ell h}_{y_0}\rangle, \tag{2.7}
$$

$$
C'_{XP}(x_0) = \left(\frac{a}{L}\right)^3 \sum_{\vec{x}} \langle \mathcal{P}^{\ell' h'}_{y_0+T_{\rm sep}} X^{h'\ell'}(\vec{x}, x_0)\rangle, \tag{2.8}
$$

where X can be either the axial current, A_0, or the pseudoscalar density, P.

For three-point correlation functions with heavy (charm or heavier) quarks we can achieve reduced statistical uncertainties by decreasing the time separation between the two sources and using smearing techniques (see Refs. [43,63]). Therefore, while in the $\bar{K}^0 - K^0$ case we have set $T_{\rm sep} = T/2$, in the $\bar{D}^0 - D^0$ case we have instead produced correlation functions setting $T_{\rm sep}/a = 18$ at $\beta = 1.9$, $T_{\rm sep}/a = 20$ at $\beta = 1.95$, and $T_{\rm sep}/a = 26$ at $\beta = 2.10$.

Estimators for the bare bag parameters are extracted from the asymptotic time behavior of the ratios of the three- to two-point correlators

$$
\begin{aligned}
\mathcal{R}^{(b)}_1(x_0) &= \frac{C_1(x_0)}{C_{AP}(x_0)C'_{AP}(x_0)},\\
\mathcal{R}^{(b)}_{i=2,\ldots,5}(x_0) &= \frac{C_{i=2,\ldots,5}(x_0)}{C_{PP}(x_0)C'_{PP}(x_0)},
\end{aligned}
\tag{2.9}
$$

which for large time separations, $y_0 \ll x_0 \ll y_0 + T_{\rm sep}$, tend to the desired (bare) bag parameters

$$
\mathcal{R}^{(b)}_1(x_0) \overset{y_0 \ll x_0 \ll y_0+T_{\rm sep}}{\longrightarrow} \left.\frac{\langle \bar{P}^0|O^{\rm MA}_{1[+]}|P^0\rangle}{\langle \bar{P}^0|A^{h\ell}_0|0\rangle\langle 0|A^{h'\ell'}_0|P^0\rangle}\right|^{(b)} \equiv B^{(b)}_1 \tag{2.10}
$$

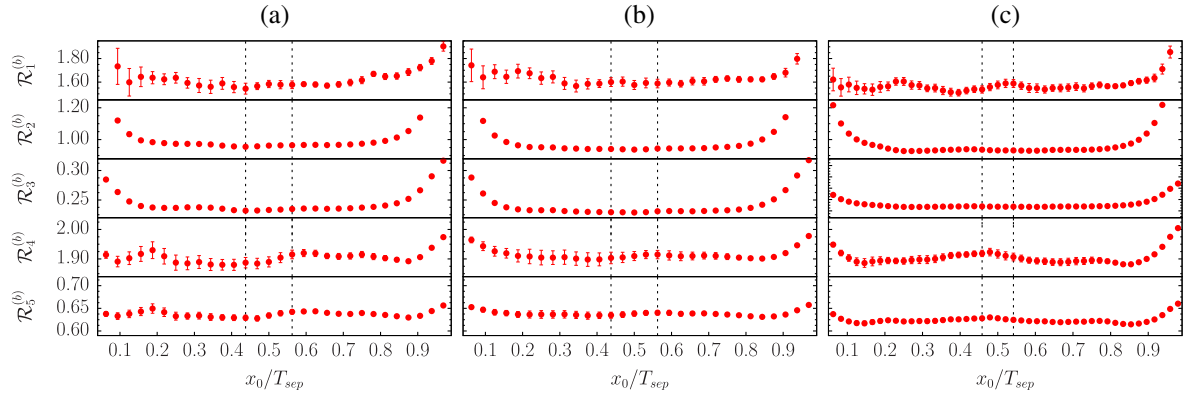

FIG. 4 (color online). $\mathcal{R}_i^{(b)}(x_0)$ $(i = 1, \ldots, 5)$ simulation points plotted against $x_0/T_{\rm sep}$ for the $\bar{K}^0 - K^0$ case: (a) $\beta = 1.90$, $(a\mu_\ell, a\mu_s) = (0.0030, 0.0185)$, volume $= 32^3 \times 64$; (b) $\beta = 1.95$, $(a\mu_\ell, a\mu_s) = (0.0025, 0.0180)$, volume $= 32^3 \times 64$; (c) $\beta = 2.10$, $(a\mu_\ell, a\mu_s) = (0.0015, 0.0151)$, volume $= 48^3 \times 96$. The dotted lines delimit the plateau region. Points for $\mathcal{R}_1^{(b)}, \ldots, \mathcal{R}_4^{(b)}$ at $\beta = 2.10$ have been slightly shifted upward by $+0.05$ for accommodating data from all three β's in the same plotting scale.

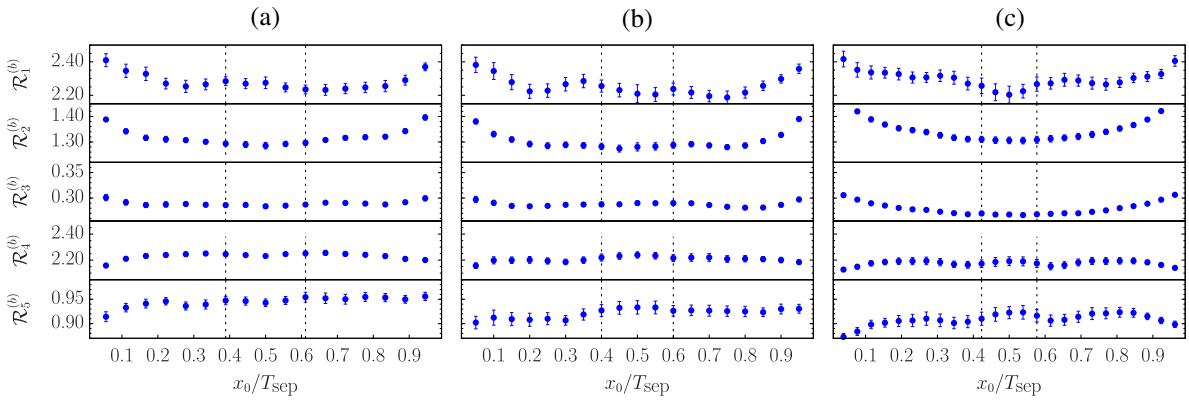

FIG. 5 (color online). $\mathcal{R}_i^{(b)}(x_0)$ $(i = 1, \ldots, 5)$ simulation points plotted against $x_0/T_{\rm sep}$ for the $\bar{D}^0 - D^0$ case: (a) $\beta = 1.90$, $(a\mu_\ell, a\mu_c) = (0.0030, 0.25)$, volume $= 32^3 \times 64$; (b) $\beta = 1.95$, $(a\mu_\ell, a\mu_c) = (0.0025, 0.22)$, volume $= 32^3 \times 64$; (c) $\beta = 2.10$, $(a\mu_\ell, a\mu_c) = (0.0015, 0.17)$, volume $= 48^3 \times 96$. The dotted lines delimit the plateau region. Points for $\mathcal{R}_1^{(b)}$ and $\mathcal{R}_2^{(b)}$ at $\beta = 2.10$ have been slightly shifted upward by $+0.1$ for accommodating data from the three β's in the same plotting scale.

$$\mathcal{R}_i^{(b)}(x_0) \overset{y_0 \ll x_0 \ll y_0 + T_{\rm sep}}{\longrightarrow} \left. \frac{\langle \bar{P}^0 | O_{i[+]}^{\rm MA} | P^0 \rangle}{\langle \bar{P}^0 | P^{h\ell} | 0 \rangle \langle 0 | P^{h'\ell'} | P^0 \rangle} \right|^{(b)} \equiv B_i^{(b)}, \quad i = 2, \ldots, 5. \tag{2.11}$$

Figures 4 and 5 refer to the neutral K and D meson cases, respectively. They illustrate the quality of the plateaux from which the estimates for the bare B_i $(i = 1, \ldots, 5)$ bag parameters are extracted. The three panels correspond to three values of the lattice spacing at which simulations were performed.

We note that our plateau choices are rather conservative and by reasonably varying the plateau interval (e.g., considering a plateau's length as long as double the size of our principal choice) we find that the maximal systematic uncertainty is at the subpercent level (with maximal estimates being 0.2% for B_2 and 0.5% for B_3 for the neutral kaon and D cases, respectively). We therefore conclude that this systematic uncertainty is so much smaller than the statistical one, indicated by the label "Stat + fit + RCs" in Tables IV and V (see below for details), that it can be safely neglected.

D. Computation of the renormalized bag parameters

The renormalization pattern of the bag parameters in our mixed action setup has been discussed in detail in Refs. [12,53,62]. The renormalized bag parameters are given by

TABLE IV. Full error budget of the $B_{1,\ldots,5}$ estimates for the neutral K-mixing.

$\bar{K}^0 - K^0$					
Source of uncertainty (%)	B_1	B_2	B_3	B_4	B_5
Stat + fit + RCs	2.5	2.4	2.7	2.7	5.4
Syst. chiral	0.8	1.3	1.1	1.8	2.6
Syst. discr.	2.0	4.7	5.8	3.8	4.1
RI′-$\overline{\text{MS}}$ matching	0.5	2.5	1.8	3.9	2.3
Total	3.4	6.0	6.7	6.3	7.6

TABLE V. Full error budget of the $B_{1,\ldots,5}$ estimates for the neutral D-mixing.

$\bar{D}^0 - D^0$					
Source of uncertainty (%)	B_1	B_2	B_3	B_4	B_5
Stat + fit + RCs	2.9	2.9	4.4	3.5	5.1
Syst. chiral	0.2	0.4	0.6	2.3	2.6
Syst. discr.	2.1	4.3	6.7	3.8	3.3
RI′-$\overline{\text{MS}}$ matching	0.5	2.5	1.7	3.9	1.1
Total	3.6	5.8	8.2	6.9	6.7

$$B_1 = \frac{Z_{11}}{\xi_1 Z_A Z_V} B_1^{(b)},$$
$$B_i = \frac{Z_{ij}}{\xi_i Z_P Z_S} B_j^{(b)} \qquad i,j = 2,\ldots,5, \tag{2.12}$$

where $(\xi_1, \xi_2, \xi_3, \xi_4, \xi_5) = (8/3, -5/3, 1/3, 2, 2/3)$. The RCs of bilinear operators, namely, Z_V, Z_A, Z_P, and Z_S, have been determined nonperturbatively in the RI′-MOM scheme in Ref. [65]. The four-fermion RCs, Z_{ij}, have also been computed nonperturbatively in the same scheme. The calculation is presented in the Appendixes A and B.

At each value of the light quark mass $\mu_\ell = \mu_{\text{sea}}$ our estimates of the bag parameters are linearly interpolated to the physical strange (for neutral K-mixing) or charm (for neutral D-mixing) quark mass. In both cases the interpolation turns out to be very smooth. A simultaneous chiral and lattice spacing extrapolation to the physical value of the pion mass and the continuum limit is finally performed. The u/d, strange and charm quark masses have been evaluated in the continuum limit in Ref. [65].

Both for neutral K and D meson mixing studies and for all the B_i's, we have employed a linear fit *Ansatz* of the general form

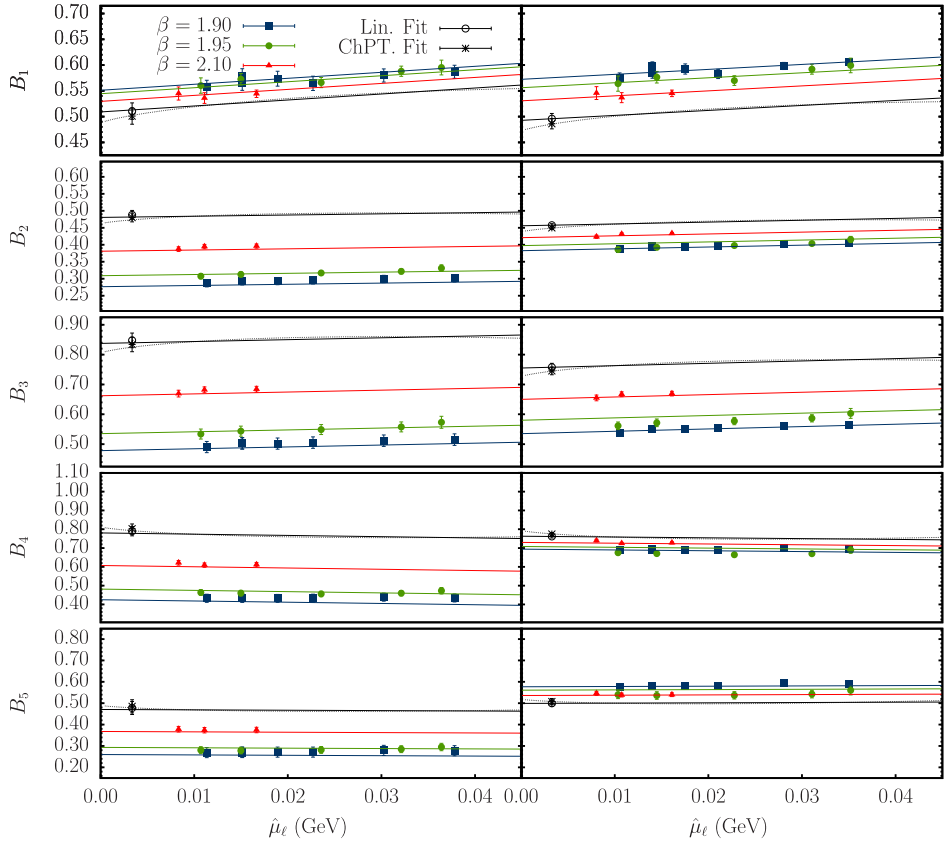

FIG. 6 (color online). Combined chiral and continuum extrapolation for the five B_i's of the $\bar{K}^0 - K^0$ case. Bag parameters are renormalized in the $\overline{\text{MS}}$ scheme of [31] at the scale of 3 GeV. Left and right panels correspond to M1-type and M2-type four-fermion RCs, respectively, following the nomenclature of Ref. [73]. In each panel open circles and stars represent the value at the physical point corresponding to the linear and NLO ChPT fits, respectively.

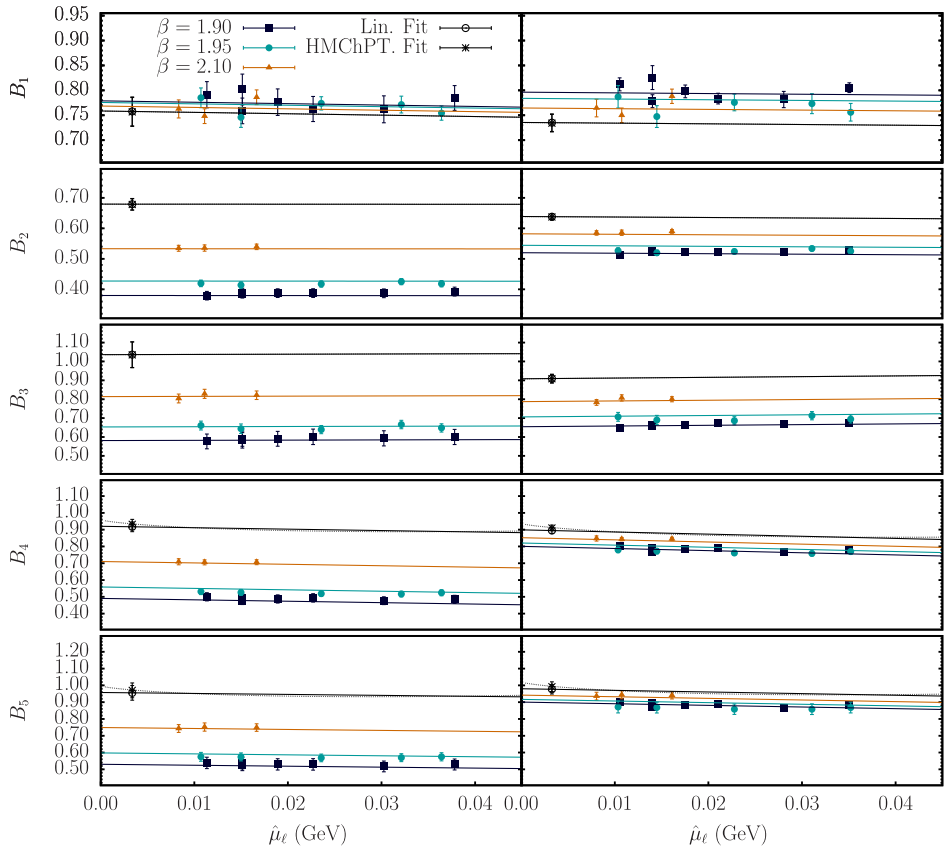

FIG. 7 (color online). Combined chiral and continuum extrapolation for the five $\bar{D}^0 - D^0$ bag parameters, B_i, renormalized in the $\overline{\text{MS}}$ scheme of [31] at the scale of 3 GeV. Left and right panels correspond to M1-type and M2-type four-fermion RCs, respectively, following the nomenclature of Ref. [73]. In each panel open circles and stars represent the value at the physical point corresponding to the linear and NLO HMChPT fit, respectively. For B_1, B_2, and B_3 the polynomial (linear) and the HMChPT fits are practically indistinguishable.

$$B_i = B_i^\chi + b_i \hat{\mu}_\ell + D_i a^2, \tag{2.13}$$

which in all cases nicely fits the data. In our notation the hat ($\hat{}$) symbol denotes renormalization in the $\overline{\text{MS}}$ scheme at the 3 GeV scale. We have also considered fit *Ansätze* based on NLO ChPT [70] for the K bag parameters, of the kind

$$B_i = \bar{B}_i^\chi \left[1 + \bar{b}_i \hat{\mu}_\ell \mp \frac{2\hat{B}_0 \hat{\mu}_\ell}{16\pi^2 f_0^2} \log \frac{2\hat{B}_0 \hat{\mu}_\ell}{16\pi^2 f_0^2} \right] + \bar{D}_i a^2 \tag{2.14}$$

and for the D bag parameters the NLO HMChPT fit *Ansätze* [71]

$$\begin{aligned} B_1 &= \tilde{B}_1^\chi \left[1 + \tilde{b}_1 \hat{\mu}_\ell - \frac{(1 - 3\hat{g}^2)}{2} \frac{2\hat{B}_0 \hat{\mu}_\ell}{16\pi^2 f_0^2} \log \frac{2\hat{B}_0 \hat{\mu}_\ell}{16\pi^2 f_0^2} \right] + \tilde{D}_1 a^2 \\ B_i &= \tilde{B}_i^\chi \left[1 + \tilde{b}_i \hat{\mu}_\ell \mp \frac{(1 \mp 3\hat{g}^2 Y)}{2} \frac{2\hat{B}_0 \hat{\mu}_\ell}{16\pi^2 f_0^2} \log \frac{2\hat{B}_0 \hat{\mu}_\ell}{16\pi^2 f_0^2} \right] + \tilde{D}_i a^2 \qquad i = 2, 4, 5. \end{aligned} \tag{2.15}$$

In Eq. (2.14) the sign in front of the logarithm is minus for $i = 1, 2, 3$ and plus for $i = 4, 5$, whereas in the second of the Eqs. (2.15) the sign is minus for $i = 2$ and plus for $i = 4, 5$. In the fit procedure we use the determinations of $\hat{B}_0$ and f_0 reported in Ref. [65]. We also make use of the value $Y = 1$ derived in Ref. [71] and of the estimate $\hat{g} = 0.53(4)$ obtained from the lattice measurement of the $g_{D^* D\pi}$ coupling [72]. In heavy quark effective theory (HQET) the bag parameter B_3 is related to B_1 and B_2. In particular, by setting $Y = 1$, B_3 and B_2 acquire identical logarithmic terms.

In Figs. 6 and 7 we display the combined chiral and continuum fit of the B_i $(i = 1, \ldots, 5)$ neutral K and D meson bag parameters renormalized in the $\overline{\text{MS}}$ scheme of Ref. [31] at the scale of 3 GeV. We report in left and right panels, respectively, data corresponding to the two ways, namely, M1 and M2, of determining the RCs proposed in Ref. [73], differing in the manner $\text{O}(a^2)$ lattice artifacts are treated. More details will be given in the Appendixes A and B. For each B_i the results using either the polynomial or the chiral fit *Ansätze* defined in Eqs. (2.13), (2.14), and (2.15) are compatible among themselves within less than 1 standard deviation. We also notice that the use of M1- and M2-type RCs, though leading to rather different discretization effects, provide compatible continuum limit determinations for the bag parameters within 1–2 standard deviations. Moreover, by comparing results from two lattice volumes, $24^3 \times 48$ and $32^3 \times 64$, at $\beta = 1.90$ at one value of the sea quark mass ($a\mu_{\text{sea}} = 0.0040$), we notice no systematic finite volume effect on the values of the bag parameters. The results for B_i agree within at most 1 standard deviation in the worst case, while for the majority of the cases they are practically indistinguishable.

III. FINAL RESULTS AND ERROR BUDGET

In this section we present the final results for the bag parameters and we discuss the error budget of statistical and systematic uncertainties.

In our analysis we combine results obtained by using several possible ways to account for systematic effects related to the RCs determination, chiral extrapolation, and discretization uncertainties. We have analyzed a number of 32 estimates for B_1 and 64 estimates for B_i with $i > 1$; see below for details.

In particular, we have examined in detail the impact on the final values of the bag parameters of various possible sources of systematic error related to the computation of the RCs. We would like to mention that a large part of the uncertainties in the RI-MOM calculation of the RCs affects the cutoff systematics in the error budget.

As described in Appendix B, we have computed the 5×5 four-fermion RCs in the RI′-MOM scheme using two different methods to deal with cutoff effects, which following Ref. [73] we label M1 and M2. The M1 method consists of removing $\text{O}((a\tilde{p})^2)$ effects in the matrix elements used to extract the RCs by performing a fit in an appreciably large fixed window of the $(a\tilde{p})^2$ momentum variable. In the M2 method the RCs are determined as weighted averages of RC estimators over a $\tilde{p}^2$-interval (fixed in physical units) and common to all the gauge configuration ensembles. To control possible systematic effects due to the choice of the momentum interval two sets of momentum intervals have been compared, leading to fully compatible results.

Note that in the mixed action setup of [53] the off-diagonal wrong chirality mixing elements of the 5×5 renormalization matrix are only $\text{O}(a^2)$ cutoff effects. If the latter are ignored, the lattice RCs matrix shows the same mixing pattern as in the formal continuum theory. To check to what extent discretization systematics can affect the final values of the bag parameters, we compared the numbers obtained by simply ignoring the off-diagonal RC matrix elements with what one gets by including $\text{O}(a^2)$ mixing effects.

The analysis of systematic uncertainties due to the use of polynomial and (HM)ChPT fit *Ansätze* [see Eqs (2.13)–(2.15)] is performed with reference to the so-called "golden" bag combinations [37]

$$G_{23} = \frac{B_2}{B_3}, \qquad G_{45} = \frac{B_4}{B_5}$$
$$G_{24} = B_2 B_4, \qquad G_{21} = \frac{B_2}{B_1}. \tag{3.1}$$

Since these quantities are constructed in a way that chiral logarithmic terms cancel up to NLO,[6] they are expected to follow an almost linear behavior as a function of $\hat{\mu}_\ell$. Using the parametrization (3.1), we obtain additional estimates for $B_{2,\ldots,5}$ without having to fit chiral logarithmic behaviors.

Finally, in order to estimate systematic uncertainties due to cutoff effects for $B_{2,\ldots,5}$, we have also carried out the scaling analysis of quantities which are found, empirically, to be affected by reduced discretization errors. Therefore, if the M1-type RCs are employed, in the K case we consider

$$B_1 \times B_2, \qquad B_2/B_3, \qquad B_3/B_4, \qquad B_4/B_5, \tag{3.2}$$

see the panels of Fig. 8, while in the D case we take

$$B_2/B_1, \qquad B_2/B_3, \qquad B_3/B_4, \qquad B_4/B_5. \tag{3.3}$$

If the M2-type RCs are employed, in the K case they are

$$B_1 \times B_2, \qquad B_1 \times B_3, \qquad B_1 \times B_4, \qquad B_1/B_5, \tag{3.4}$$

while in the D case we take

$$B_1 \times B_2, \qquad B_1 \times B_3, \qquad B_1 \times B_4, \qquad B_1 \times B_5. \tag{3.5}$$

Naturally in this kind of analysis all the BSM bag parameters will eventually turn out to be expressed in terms of B_1 which, however, among all the others is the quantity that is least affected by discretization effects.

[6]Strictly speaking in the case of D this is not so for the combination G_{24} as the NLO logarithmic terms do not cancel out completely. However, since the G_{24} data show anyway a good linear behavior vs the light quark mass, we tried a linear fit *Ansatz* even in this case.

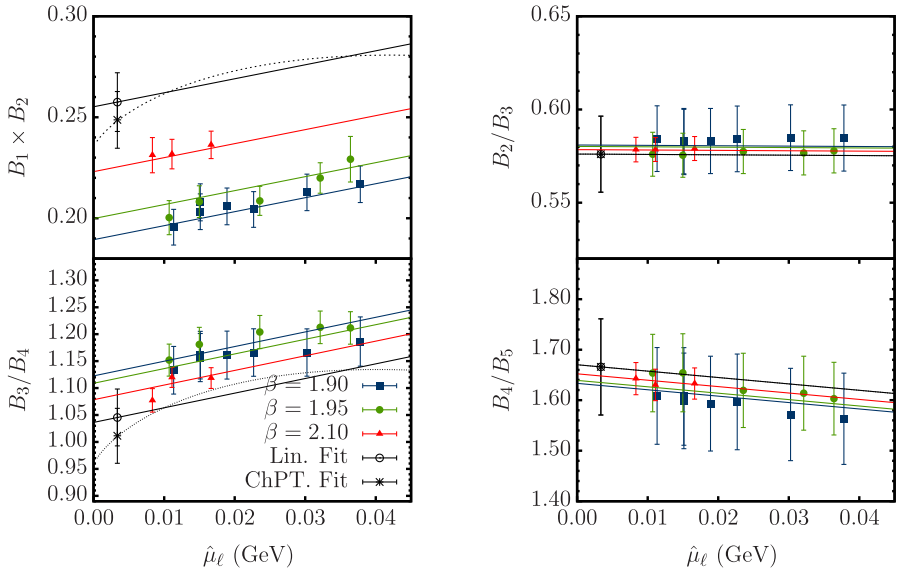

FIG. 8 (color online). Combined chiral and continuum extrapolation in the $\bar{K}^0 - K^0$ case of the combinations defined in Eq. (3.2). We use M1-type RCs in the $\overline{\text{MS}}$ scheme of [31] at 3 GeV. For the combinations shown in the right panels the polynomial (linear) and the NLO ChPT fit *Ansätze* coincide.

To summarize we have carried out[7] 32 kinds of analysis for B_1 and 64 for the BSM bag parameters, $B_{2,\ldots,5}$.

Statistical errors have been evaluated using the jackknife method. We have verified that for all the gauge configuration ensembles 16 jackknife bins are enough to have autocorrelations well under control. Fit cross correlations are taken into account by generating 1000 bootstrap samples for each gauge configuration ensemble. The RC computation has been performed on a different set of $N_f = 4$ gauge configuration ensembles. The error on each RC has been propagated assuming RCs to be Gaussian distributed with the central values and the standard deviations reported in Tables VII and IX.

Our total statistical uncertainty includes the statistical errors on the bare matrix elements, the statistical uncertainty of the RCs, and the propagated error coming from the combined continuum and chiral fit extrapolation.

For each bag parameter the central value is determined by the average over the corresponding set of results. Note that, since all our analyses are characterized by comparable fit quality, we combine the results from different analyses assuming the same weight for all of them. Therefore for the final central values as well as for the statistical and systematic uncertainties, we make use of the formulas (as already done in Ref. [65])

$$\bar{x} = \frac{1}{N}\sum_{i=1}^{N} x_i, \tag{3.6}$$

$$\sigma^2 = \frac{1}{N}\sum_{i=1}^{N} \sigma_i^2 + \frac{1}{N}\sum_{i=1}^{N} (x_i - \bar{x})^2, \tag{3.7}$$

where x_i and σ_i are the central value and the variance of the ith analysis and N is the total number of analyses, i.e., $N = 32$ for B_1 and $N = 64$ for $B_{2,\ldots,5}$. From the first term of the rhs of Eq. (3.7) we read off the statistical error while the second, which represents the spread among the results of different analyses, provides an estimate for the total systematic uncertainty.

In Tables I and II we have collected our final results for B_i $(i = 1, \ldots, 5)$ evaluated in the $\overline{\text{MS}}$ and RI′ schemes. The final uncertainty is given by summing in quadrature the statistical and the systematic errors following Eq. (3.7).

In Figs. 9 and 10 we illustrate the distribution of the results for each B_i in the K and D case, respectively. Had we chosen the median of the results to represent the central value, we would have obtained numbers fully compatible (within better than 1 statistical standard deviation) with the results collected in Tables I and II. It has also been checked that the width of the interval which selects the 68% of the area around the average (or the median) is in all cases very

[7]The total number of different analyses for the SM bag parameter B_1 we have considered is given by the product $32 = 2 \times 4 \times 2 \times 2$. These numbers refer to the two fit *Ansätze* for the chiral extrapolation, the four ways of combining the M1 and M2 kinds of RC estimates needed for the renormalization of the four- and two-fermion operators, the two choices of the p^2-interval, and finally a factor of 2 for including the off-diagonal scale-independent $O(a^2)$ matrix elements Δ_{ij} in the construction of the renormalized operators or setting them equal to zero. As for the number of BSM bag-parameter analyses, owing to the alternative ways of parametrizing chiral [Eq. (3.1)] and lattice spacing fit *Ansätze* [Eqs. (3.2), (3.4) and Eqs. (3.3), (3.5)], the above number must be multiplied by 2, thus giving in total 64 kinds of analysis.

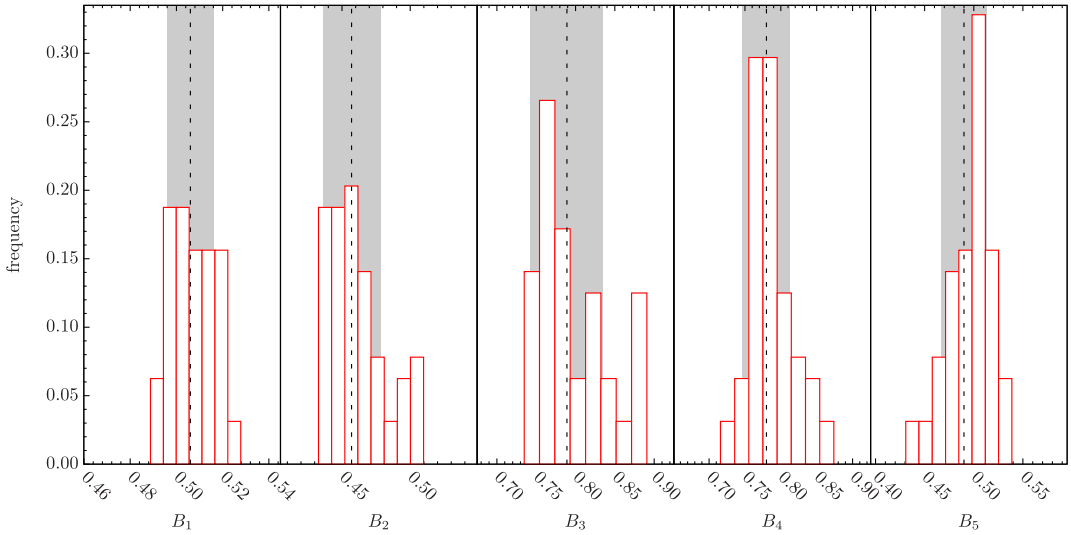

FIG. 9 (color online). Distribution of $B_{1,\ldots,5}$ results for the neutral K-mixing renormalized in the $\overline{\text{MS}}$ scheme of Ref. [31] at the scale of 3 GeV. The solid vertical line marks the central value (average) while the gray band indicates the systematic error determined from Eq. (3.7).

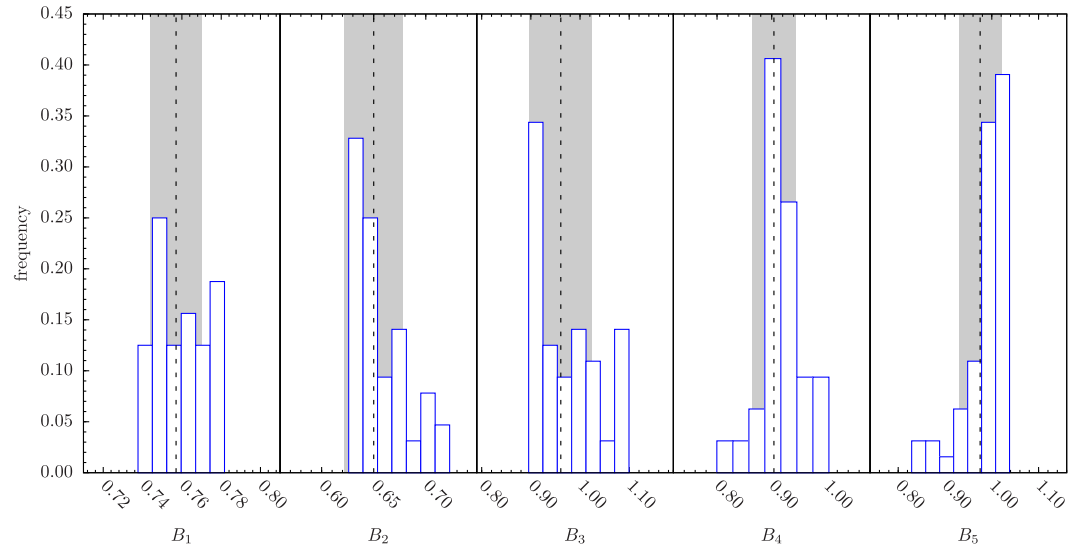

FIG. 10 (color online). Same as in Fig. 9 but for the neutral D-mixing.

close to the value provided by Eq. (3.7). We consider this a nice test of the validity and usefulness of our way of estimating the total error.[8]

In Tables IV and V we report the detailed error budget of our determination of the K and D bag parameters. The numbers represent the percentage of the main sources of uncertainty in our calculation. The total percentage error is reported in the last rows of Tables IV and V.

Under the label "Stat + fit + RCs" we lump together the error coming from the statistical uncertainties of correlators, the interpolation/extrapolation of the simulated quark masses to the physical values, the extrapolation to the continuum limit, and the statistical uncertainties of the RCs.

Under the label "Syst. chiral" we give our estimates of the chiral fit uncertainty. This has been determined using the different ways we have used to perform the chiral

[8]The fit quality for the vast majority of the 32 analyses for B_1 and the 64 analyses for $B_{i=2,\ldots,5}$ is good, while only for a small number of cases—in particular, 6 (7) out of 64 analyses for B_2 and 10 (11) out of 64 analyses for B_4 for the neutral kaon (D) case—did we notice poor fit quality. Nevertheless, we decided to attribute to the results of all analyses the same weight since this choice led to somewhat more conservative estimates of the systematic uncertainties. In fact if we had opted for a χ^2-weighted analysis strategy, the shifts of the central values for all B_i would have been minimal and the final estimated systematic errors would have been smaller (by a few percent for $B_{i=1,2,4}$ up to almost 30% for $B_{i=3,5}$) than the ones presented in Tables IV and V.

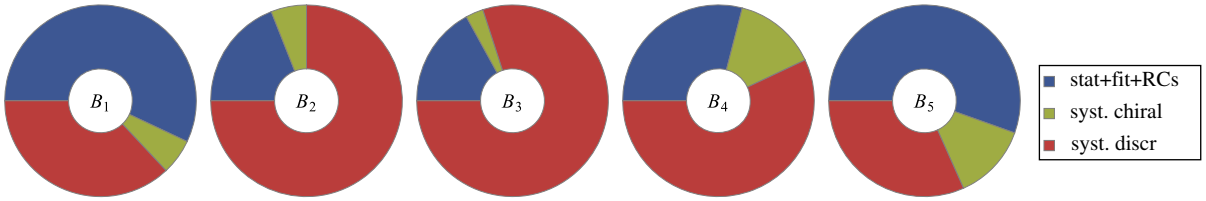

FIG. 11 (color online). Graphical representation of the error budget owing to the lattice computation (i.e., without including the estimate for the systematic uncertainty due to the perturbative matching between the RI′ and $\overline{\text{MS}}$ schemes) for the K bag parameters, as reported in Table IV.

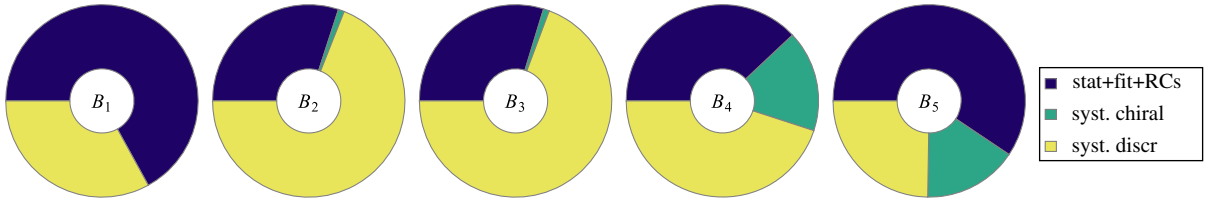

FIG. 12 (color online). Same as in Fig. 11 for the D bag parameters.

extrapolation, namely, comparing results coming from the use of Eqs. (2.13), (2.14), and (2.15) as well as Eqs. (3.1).

In the row labeled "Syst. discr." we give our final estimate of the systematic uncertainties related to the choice of the fit *Ansatz* of discretization artifacts. The uncertainty is taken as the spread of the bag parameter results obtained with the use of Eqs. (3.2) to (3.5) and of the different ways (M1 or M2) of computing the relevant RCs.

Finally, in the last row of each table we quote our estimate for the systematic uncertainty due to the perturbative matching of the RI′ and $\overline{\text{MS}}$ schemes. We recall that anomalous dimensions of the four-fermion operators are known up to NLO. Our associated systematic error has been estimated by considering the difference between the values obtained at NLO and LO at the scale of 3 GeV for each one of the bag parameters and multiplying it with the value ($\sim$0.25) that $\alpha_s^{\overline{\text{MS}}}(3\ \text{GeV})$ takes at the same scale.

Finite volume effects, as mentioned in the previous section, are practically negligible at the level of our precision.

In Figs. 11 and 12 we graphically show the error budget associated to the lattice computation, i.e., without including the systematic error due to the perturbative conversion from the RI′ to $\overline{\text{MS}}$ scheme; see Tables IV and V.

ACKNOWLEDGMENTS

We warmly thank our colleagues of the ETM Collaboration for fruitful discussions. We acknowledge the CPU time provided by the PRACE Research Infrastructure under the projects PRA027 "QCD Simulations for Flavor Physics in the Standard Model and Beyond" and PRA067 "First Lattice QCD Study of B-physics with Four Flavors of Dynamical Quarks" on the BG/P and BG/Q systems at the Jülich SuperComputing Center (Germany) and at CINECA (Italy), and by the agreement between INFN and CINECA under the specific initiative INFN-LQCD123 on the Fermi BG/Q system at CINECA (Italy). V. L., S. S., and C. T. thank MIUR (Italy) for partial support under Contract No. PRIN 2010-2011.

APPENDIX A: COMPUTATIONAL SETUP FOR THE RCs

As we use a mass-independent renormalization scheme, the calculation of the RCs of two- and four-fermion operators and in particular of operators with nonvanishing anomalous dimension must be performed in the massless quark limit.

For this purpose we have produced dedicated sets of $N_f = 4$ Wilson twisted-mass degenerate dynamical quark gauge configurations with the same gluon action as the one used in the nondegenerate case and for a number of moderately light sea masses. For each ensemble with given sea quark mass parameters we have also computed the RC estimators at several values of the valence parameters. Naturally the RCs computed with either $N_f = 2 + 1 + 1$ or $N_f = 4$ ensembles would yield identical numbers in the chiral limit.

The $N_f = 4$ ensembles are generated at values of the twist angle somewhat different from $\pi/2$ (maximal twist), i.e., at $m_0 \neq m_{\text{cr}}$. The reason is that for small values of $m_0 - m_{\text{cr}}$ large autocorrelation times have been noticed for simulations performed at two out of the three values of the inverse gauge coupling ($\beta = 1.90$ and 1.95) that we use. Although an off-maximal-twist setup does not lead to automatic $\text{O}(a)$ improvement, one can prove [54] that for any hadronic observable the average over results obtained at opposite values of the PCAC quark mass is actually $\text{O}(a)$ improved. Naturally, the need for performing

the average leads to doubling the CPU time cost of the calculation, which however remains quite affordable as we are dealing with simulations at nonzero standard Wilson and twisted mass.

In Appendix A of Ref. [65] we have presented in detail the $N_f = 4$ operator renormalization procedure for the cases of quark field and quark bilinears. Nevertheless, for the reader's convenience and to fix our notations, we briefly summarize here the main parts of our $N_f = 4$ computational setup.

We employ the Iwasaki action for the gluons while the $N_f = 4$ fermionic action in the so-called twisted basis reads

$$S_{tm}^{\rm sea} = a^4 \sum_{x,f} \bar{\chi}_f^{\rm sea} [\gamma \cdot \tilde{\nabla} + W_{\rm cr} + (m_{0,f}^{\rm sea} - m_{\rm cr}) + i r_f^{\rm sea} \mu_f^{\rm sea} \gamma_5] \chi_f^{\rm sea}, \tag{A1}$$

where $f = u, d, s, c$; $\gamma \cdot \tilde{\nabla} = \gamma_\mu (\nabla_\mu + \nabla_\mu^*)/2$; and $W_{\rm cr} = -(a/2)\nabla_\mu^* \nabla_\mu + m_{\rm cr}$. We have also set

$$r_d^{\rm sea} = -r_u^{\rm sea}, \qquad r_c^{\rm sea} = -r_s^{\rm sea}$$
$$\mu_u^{\rm sea} = \mu_d^{\rm sea} = \mu_s^{\rm sea} = \mu_c^{\rm sea} \equiv \mu^{\rm sea}. \tag{A2}$$

Note that the form of the action (A2) guarantees the positivity of the fermion determinant. The valence fermion action takes the form

$$S^{\rm val} = a^4 \sum_{x,f} \bar{\chi}_f^{\rm val} [\gamma \cdot \tilde{\nabla} - \frac{a}{2} \nabla_\mu^* \nabla_\mu + m_{0,f}^{\rm val} + i r_f^{\rm val} \mu_f^{\rm val} \gamma_5] \chi_f^{\rm val}. \tag{A3}$$

In our notations the sea and valence sectors of the various $r_f^{\rm val,sea}$-Wilson parameters take values equal to ± 1 and the twisted masses $a\mu_f^{\rm val,sea}$ are non-negative quantities.

In Table VI we report the simulation details and the quark mass parameters relevant for the $N_f = 4$ gauge ensembles defined above. For each value of the sea (twisted) quark mass, $a\mu^{\rm sea}$, we have generated two gauge ensembles which are denoted by the letter "m" or "p" added to their label, and correspond to (nearly) opposite values of the PCAC quark mass, $am_{\rm PCAC}^{\rm sea}$.

Moreover, for each of the sea gauge ensembles, quark propagators have been computed for a number of valence quark twisted masses, $a\mu^{\rm val}$. The measured value of the

TABLE VI. Simulation details and quark mass parameters of the $N_f = 4$ gauge ensembles employed in the RC computation.

	$a\mu^{\rm sea}$	$am_{\rm PCAC}^{\rm sea}$	$am_0^{\rm sea}$	$\theta^{\rm sea}$	$a\mu^{\rm val}$	$am_{\rm PCAC}^{\rm val}$
			$\beta = 1.90$ ($L = 24$, $T = 48$)			
A4m	0.0080	−0.0390(01)	0.0285(01)	−1.286(01)	{0.0060, 0.0080, 0.0120,	−0.0142(02)
A4p		0.0398(01)	0.0290(01)	+1.291(01)	0.0170, 0.0210, 0.0260}	+0.0147(02)
A3m	0.0080	−0.0358(02)	0.0263(01)	−1.262(02)	{0.0060, 0.0080, 0.0120,	−0.0152(02)
A3p		0.0356(02)	0.0262(01)	+1.260(02)	0.0170, 0.0210, 0.0260}	+0.0147(03)
A2m	0.0080	−0.0318(01)	0.0237(01)	−1.226(02)	{0.0060, 0.0080, 0.0120,	−0.0155(02)
A2p		+0.0310(02)	0.0231(01)	+1.218(02)	0.0170, 0.021 0, 0.0260}	+0.0154(02)
A1m	0.0080	−0.0273(02)	0.0207(01)	−1.174(03)	{0.0060, 0.0080, 0.0120,	−0.0163(02)
A1p		+0.0275(04)	0.0209(01)	+1.177(05)	0.0170, 0.021 0, 0.0260}	+0.0159(02)
			$\beta = 1.95$ ($L = 24$, $T = 48$)			
B1m	0.0085	−0.0413(02)	0.0329(01)	−1.309(01)	{0.0085, 0.0150, 0.0203,	−0.0216(02)
B1p		+0.0425(02)	0.0338(01)	+1.317(01)	0.0252, 0.02 98}	+0.0195(02)
B7m	0.0085	−0.0353(01)	0.0285(01)	−1.268(01)	{0.0085, 0.0150, 0.0203,	−0.0180(02)
B7p		+0.0361(01)	0.0285(01)	+1.268(01)	0.0252, 0.02 98}	+0.0181(01)
B8m	0.0020	−0.0363(01)	0.0280(01)	−1.499(01)	{0.0085, 0.0150, 0.0203,	−0.0194(01)
B8p		+0.0363(01)	0.0274(01)	+1.498(01)	0.0252, 0.02 98}	+0.0183(02)
B3m	0.0180	−0.0160(02)	0.0218(01)	−0.601(06)	{0.0060, 0.0085, 0.0120, 0.0150,	−0.0160(02)
B3p		+0.0163(02)	0.0219(01)	+0.610(06)	0.0180, 0.0203, 0.0252, 0.0298}	+0.0162(02)
B2m	0.0085	−0.0209(02)	0.0182(01)	−1.085(03)	{0.0085, 0.0150, 0.0203,	−0.0213(02)
B2p		+0.0191(02)	0.0170(02)	+1.046(06)	0.0252, 0.02 98}	+0.0191(02)
B4m	0.0085	−0.0146(02)	0.0141(01)	−0.923(04)	{0.0060, 0.0085, 0.0120, 0.0150,	−0.0146(02)
B4p		+0.0151(02)	0.0144(01)	+0.940(07)	0.0180, 0.0203, 0.0252, 0.0298}	+0.0151(02)
			$\beta = 2.10$ ($L = 32$, $T = 64$)			
C5m	0.0078	−0.00821(11)	0.0102(01)	−0.700(07)	{0.0048, 0.0078, 0.0119,	−0.0082(01)
C5p		+0.00823(08)	0.0102(01)	+0.701(05)	0.0190, 0.0242, 0.0293}	+0.0082(01)
C4m	0.0064	−0.00682(13)	0.0084(01)	−0.706(09)	{0.0039, 0.0078, 0.0119,	−0.0068(01)
C4p		+0.00685(12)	0.0084(01)	+0.708(09)	0.0190,0.0242, 0.0293}	+0.0069(01)
C3m	0.0046	−0.00585(08)	0.0066(01)	−0.794(07)	{0.0025, 0.0046, 0.0090, 0.0152,	−0.0059(01)
C3p		+0.00559(14)	0.0064(01)	+0.771(13)	0.0201, 0.0249, 0.0297}	+0.0056(01)
C2m	0.0030	−0.00403(14)	0.0044(01)	−0.821(17)	{0.0013, 0.0030, 0.0080, 0.0143,	−0.0040(01)
C2p		+0.00421(13)	0.0045(01)	+0.843(15)	0.0195, 0.0247, 0.0298}	+0.0042(01)

valence PCAC quark mass, $am^{\rm val}_{\rm PCAC}$, for each sea ensemble of the "m" or "p" type is given in the last column of Table VI.

Based on Ref. [53] the definition of the renormalized quark mass parameters in our partially quenched setup is

$$\mathcal{M}^{\rm sea,val} = Z_P^{-1}\mathcal{M}_0^{\rm sea,val} = Z_P^{-1}\sqrt{(Z_A m_{\rm PCAC}^{\rm sea,val})^2 + (\mu^{\rm sea,val})^2},$$
$$\mathrm{tg}\theta_f^{\rm sea,val} = \frac{Z_A m_{\rm PCAC}^{\rm sea,val}}{r_f^{\rm sea,val}\mu^{\rm sea,val}}, \tag{A4}$$

where Z_A is the RC of the (flavor nonsinglet) axial current and $m_{\rm PCAC}^{\rm sea,val}$ denotes the PCAC quark mass computed from correlators in the sea and valence sector, respectively. The angles $\theta_f^{\rm sea}$ and $\theta_f^{\rm val}$ are determined from the formulas $\mathcal{M}^{\rm sea/val}\cos(\theta_f^{\rm sea/val}) = r_f^{\rm sea/val}\mu^{\rm sea/val}$ and $\mathcal{M}^{\rm sea/val}\sin(\theta_f^{\rm sea/val}) = Z_A m_{\rm PCAC}^{\rm sea/val}$, respectively. If convenient, quark mass parameters in the valence sector may be chosen to be different from their sea counterparts.

Our RC estimators are evaluated at the values $p_\mu = (2\pi/L_\mu)n_\mu$ of the momenta, where

$$n_\mu = ([0,2],[0,2],[0,2],[0,3])([2,3],[2,3],[2,3],[4,7]), \quad \text{for } \beta = 1.95,$$
$$n_\mu = ([0,2],[0,2],[0,2],[0,3])([2,5],[2,5],[2,5],[4,9]), \quad \text{for } \beta = 1.90 \quad \text{and} \quad 2.10 \tag{A5}$$

with L_μ the lattice size along the direction μ (with $L_4 \equiv T$ and $L_{1,2,3} \equiv L$). Quark fields obey antiperiodic time boundary conditions implemented by a constant shift, $\Delta p_4 = \pi/L_4$, in the time component of the four-momentum. Notice also that our final analysis of the RC estimators has been carried out using "democratic" four-momentum values that satisfy the condition

$$\Delta_4(p) \equiv \frac{\sum_\mu \tilde{p}_\mu^4}{(\sum_\mu \tilde{p}_\mu^2)^2} < 0.29, \tag{A6}$$

with

$$\tilde{p}_\mu \equiv \frac{1}{a}\sin(a p_\mu). \tag{A7}$$

In order to come up with smoother discretization errors we have subtracted from the Green's functions entering the RI-MOM computation the perturbative cutoff effects up to order $O(a^2 g^2)$ (see Refs. [74,75]).

As it has been stated above, following the general proof given in Ref. [54], which in Appendix A. 2 of Ref. [65] has been exemplified for the case of quark bilinear RC estimators, the average over RC estimators computed on ensembles produced with opposite values of the sea and valence PCAC quark mass enables us to remove all the odd integer power cutoff effects and hence the $\mathcal{O}(a)$ discretization errors.[9] Based on the definition of the angle θ in terms of the PCAC quark mass given in Eq. (A4), we generally refer to this procedure as θ-average O(a) improvement.

The evaluation of the RCs for the quark bilinear operators, namely, Z_A, Z_V, Z_P, and Z_S, as well as the RC of the quark wave function, Z_q, has been done in Ref. [65]. Our final numbers at each value of β have been labeled as M1 or M2 RCs. As explained in detail in [65], they correspond to different ways in which the cutoff effects are treated. For convenience all the results are again reported in Table VII of Appendix B of the present work. Note that as for Z_V, in the present analysis we have made use of the much more precise Ward-Takahashi identity determination [73].

APPENDIX B: RI-MOM COMPUTATION OF RCs OF THE FOUR-FERMION OPERATORS

The RI′-MOM renormalization procedure we used for the four-fermion operators has been explained in Appendixes A and B of Ref. [12]. From the conceptual and operational point of view, a great part of the computational details are very similar between the $N_f = 2$ case of Ref. [12] and the present $N_f = 4$ case, except for the fact that in the latter one has to compute RC estimators in the "m" and "p" ensembles separately before taking their θ-average. In this section we will fix our notations by making extensive use of the description of Ref. [12]. We will however recall some essential points of the computation in order to make it easier for the reader to follow the presentation of the analysis and our results.

In computing RCs it is convenient to work in a basis where the operators $O^{\rm MA}_{i[\pm]}$, with $i = 2,\ldots,5$ defined in Eq. (2.4), are Fierz transformed as suggested in Ref. [76]. Using here a generic labeling [that can be obviously adapted to the case of interest $(1,2,3,4) \to (h,\ell,h',\ell')$] the operator basis now reads[10]

[9]The proof for the case of the RCs of the four-fermion operators required in our mixed action setup (see Sec. II C) is closely analogous to the one for the case of quark bilinear RCs.

[10]The quark fields q_1, q_2, q_3, and q_4 are valence fields with the lattice action specified in Eq. (2.3); i.e., they are written in the physical basis of maximally twisted LQCD.

$$
\begin{aligned}
Q^{\mathrm{MA}}_{1[\pm]} &= 2\{([\bar{q}_1\gamma_\mu q_2][\bar{q}_3\gamma_\mu q_4] + [\bar{q}_1\gamma_\mu\gamma_5 q_2][\bar{q}_3\gamma_\mu\gamma_5 q_4]) \pm (2 \leftrightarrow 4)\} \\
Q^{\mathrm{MA}}_{2[\pm]} &= 2\{([\bar{q}_1\gamma_\mu q_2][\bar{q}_3\gamma_\mu q_4] - [\bar{q}_1\gamma_\mu\gamma_5 q_2][\bar{q}_3\gamma_\mu\gamma_5 q_4]) \pm (2 \leftrightarrow 4)\} \\
Q^{\mathrm{MA}}_{3[\pm]} &= 2\{([\bar{q}_1 q_2][\bar{q}_3 q_4] - [\bar{q}_1\gamma_5 q_2][\bar{q}_3\gamma_5 q_4]) \pm (2 \leftrightarrow 4)\} \\
Q^{\mathrm{MA}}_{4[\pm]} &= 2\{([\bar{q}_1 q_2][\bar{q}_3 q_4] + [\bar{q}_1\gamma_5 q_2][\bar{q}_3\gamma_5 q_4]) \pm (2 \leftrightarrow 4)\} \\
Q^{\mathrm{MA}}_{5[\pm]} &= 2\{([\bar{q}_1\sigma_{\mu\nu} q_2][\bar{q}_3\sigma_{\mu\nu} q_4]) \pm (2 \leftrightarrow 4)\} \quad (\text{for } \mu > \nu),
\end{aligned}
\tag{B1}
$$

where color indices are meant to be contracted within each square parenthesis, "MA" stands for "mixed action," and $\sigma_{\mu\nu} = [\gamma_\mu, \gamma_\nu]/2$. The transformation matrix between the two operator bases [Eqs. (2.4) and (B1)] is given by

$$
O^{\mathrm{MA}}_{i[\pm]} = \Lambda^{[\pm]}_{ij} Q^{\mathrm{MA}}_{j[\pm]}, \qquad \Lambda^{[\pm]} = \begin{pmatrix} 1 & 0 & 0 & 0 & 0 \\ 0 & 0 & 0 & 1 & 0 \\ 0 & 0 & 0 & \mp 1/2 & \pm 1/2 \\ 0 & 0 & 1 & 0 & 0 \\ 0 & \mp 1/2 & 0 & 0 & 0 \end{pmatrix}. \tag{B2}
$$

To simplify the notation, in the rest of the Appendix we drop the superscript "MA" and subscript "±" and denote the operators (B1) simply with the symbol Q_i. Then in a self-evident matrix notation the renormalization pattern of the bare operators $\mathbf{Q}^{(b)}$ takes the form

$$
\mathbf{Q}^{\mathrm{ren}} = \mathbf{Z_Q}[\mathbf{I} + \mathbf{\Delta}]\mathbf{Q}^{(b)}, \tag{B3}
$$

where $\mathbf{Z_Q}$ is a scale-dependent renormalization matrix which has the same block-diagonal form as the formal continuum one. The wrong chirality mixings are parametrized by $\mathbf{\Delta}$ which is a sparse off-diagonal and UV-finite matrix with the structure

$$
\mathbf{\Delta} = \begin{bmatrix} 0 & \Delta_{12} & \Delta_{13} & \Delta_{14} & \Delta_{15} \\ \Delta_{21} & 0 & 0 & \Delta_{24} & \Delta_{25} \\ \Delta_{31} & 0 & 0 & \Delta_{34} & \Delta_{35} \\ \Delta_{41} & \Delta_{42} & \Delta_{43} & 0 & 0 \\ \Delta_{51} & \Delta_{52} & \Delta_{53} & 0 & 0 \end{bmatrix}. \tag{B4}
$$

The renormalization pattern (B3) can be proved (following Appendix A of Ref. [12]) for the renormalization of $\mathbf{Q}$ defined out of maximal twist, for both positive and negative m_{PCAC} masses—we refer to the ensembles "p" and "m" discussed in the previous appendix. At this level of course lattice artifacts are still $\mathrm{O}(a)$. By the θ-averaging procedure discussed above, however, we obtain $\mathrm{O}(a)$ improved RC estimators for which Eq. (B3) holds with only $\mathrm{O}(a^2)$ lattice artifacts. These RC estimators are used for renormalizing the bare matrix element we computed at maximal twist.

For completeness we summarize the main technical points of the RC calculations. We start by computing in the Landau gauge the four-point Green's function of the operators, Q_i, between external quark states with the momenta given in Eqs. (A5)–(A7).

The RI′-MOM renormalization condition is imposed by requiring the projected amputated functions be equal to their tree-level value. This last step is conveniently and compactly implemented with the construction of the so-called dynamic matrix defined by the equation $\mathbf{D} = \mathbf{P\Lambda}$, where $\mathbf{P}$ and $\mathbf{\Lambda}$ are the matrices of the spin projectors and the amputated Green's functions, respectively; see also Appendix B. 1 of Ref. [12].

The further steps of the analysis are the following.

(i) We subtract from the dynamic matrix and the quark form factor (relevant for Z_q) the perturbative $\mathrm{O}(a^2 g^2_{\mathrm{boost}})$ corrections computed in the massless theory [74,75]. The boosted coupling is defined as $g^2_{\mathrm{boost}} = 6/(\beta\langle P\rangle)$, where $\langle P\rangle$ is the average plaquette value.

(ii) We subtract from the projected amputated four-fermion correlators the contribution of the Goldstone boson (GB) pole at each value of the momenta defined in Eqs. (A5)–(A7). This step is performed by carrying out the chiral limit extrapolation in the valence sector. The GB pole contribution is realized by the presence of terms that go as[11] $(1/m^2_{ps})^n$, each one of them being suppressed by corresponding powers of the inverse square momentum, $(1/\tilde{p}^2)^n$. For each sea quark ensemble and for each value of the momentum, we fit each one of the dynamic matrix elements in terms of the pseudoscalar mass in the valence sector, using the *Ansatz*

[11]For each combination of two valence quark masses in each gauge ensemble of Table VI we have computed and used the corresponding value of the pseudoscalar mass, m_{ps}.

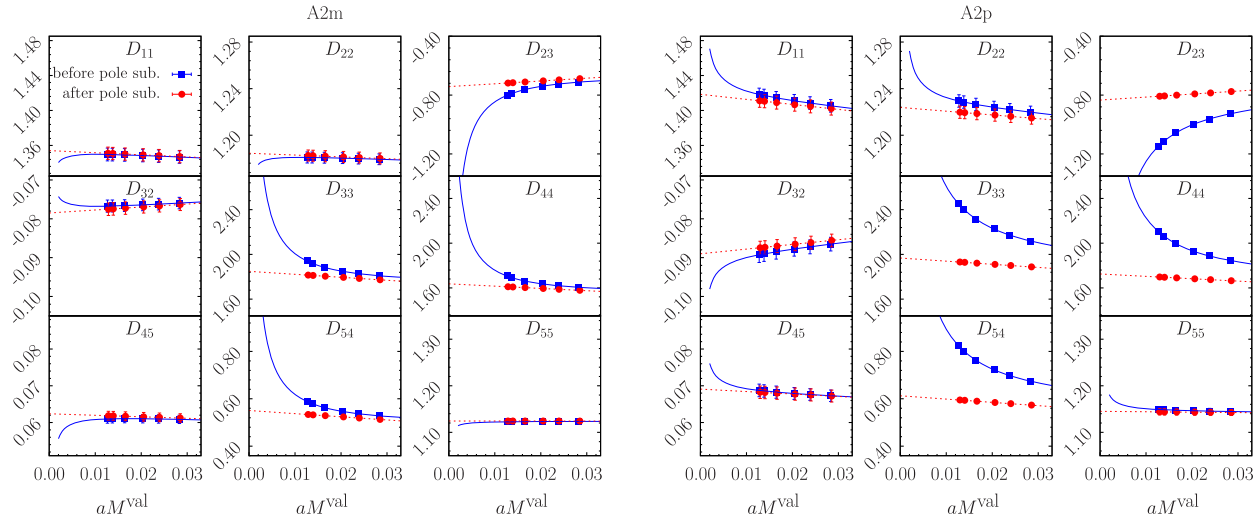

FIG. 13 (color online). Fitting procedure for the GB pole subtraction on the block-diagonal elements of the dynamic matrix. We show two examples from the coarsest lattice, in particular for the ensembles A2m (left) and A2p (right), at a relatively small value of momentum, namely, $(a\tilde{p})^2 \simeq 1.57$.

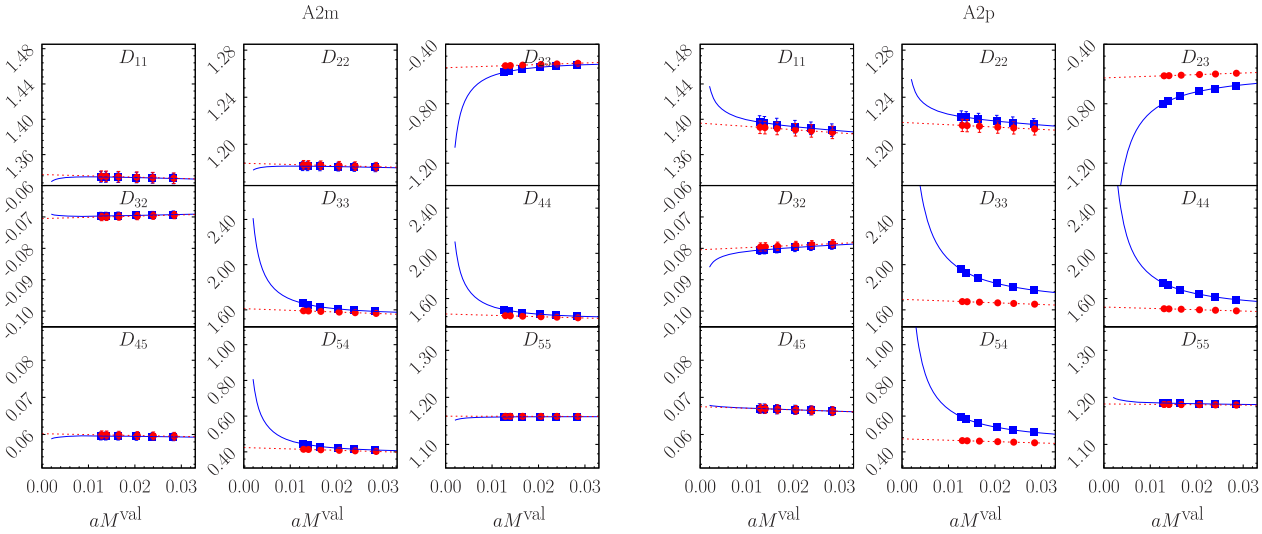

FIG. 14 (color online). Same as in Fig. 13 but at a larger value of momentum, namely, $(a\tilde{p})^2 \simeq 2.19$.

$$D_{ij}(a^2\tilde{p}^2; m_{ps}^2) = \mathcal{A}(a^2\tilde{p}^2) + \mathcal{B}(a^2\tilde{p}^2)m_{ps}^2 + \mathcal{C}(a^2\tilde{p}^2)/m_{ps}^2 + \mathcal{D}(a^2\tilde{p}^2)/(m_{ps}^2)^2. \quad \text{(B5)}$$

In Fig. 13 we show the GB pole subtraction of the block-diagonal elements of the dynamic matrix corresponding to the continuumlike matrix elements in the case of the coarsest lattice ($\beta = 1.90$) at relatively small momenta where systematic effects are expected to be larger. We observe, as it is also expected, that the GB pole contribution is getting suppressed as the value of the momentum increases. This feature can be noticed while comparing Figs. 13 and 14, as both refer to $\beta = 1.90$ at two different values of the momentum. Moreover, typical GB pole subtraction fits in the finest lattice are given in the panels of Fig. 15.

Important information concerning the double GB pole subtraction can be revealed from plots as, for example, those presented in the panels of Fig. 16, which refer to the ensembles A1p and A1m of the coarsest lattice spacing ($\beta = 1.90$). We form the product of $(a^2\tilde{p}^2)^2$ with the fit parameter, $\mathcal{D}(a^2\tilde{p}^2)$, of the double GB pole term [cf. Eq. (B5)] and then plot it against $(a^2\tilde{p}^2)$. Two observations are in order. First, we notice that the product $\mathcal{D}(a^2\tilde{p}^2) \times (a^2\tilde{p}^2)^2$ takes almost constant value for large enough values of momentum that lie in the momentum intervals we have used in order to

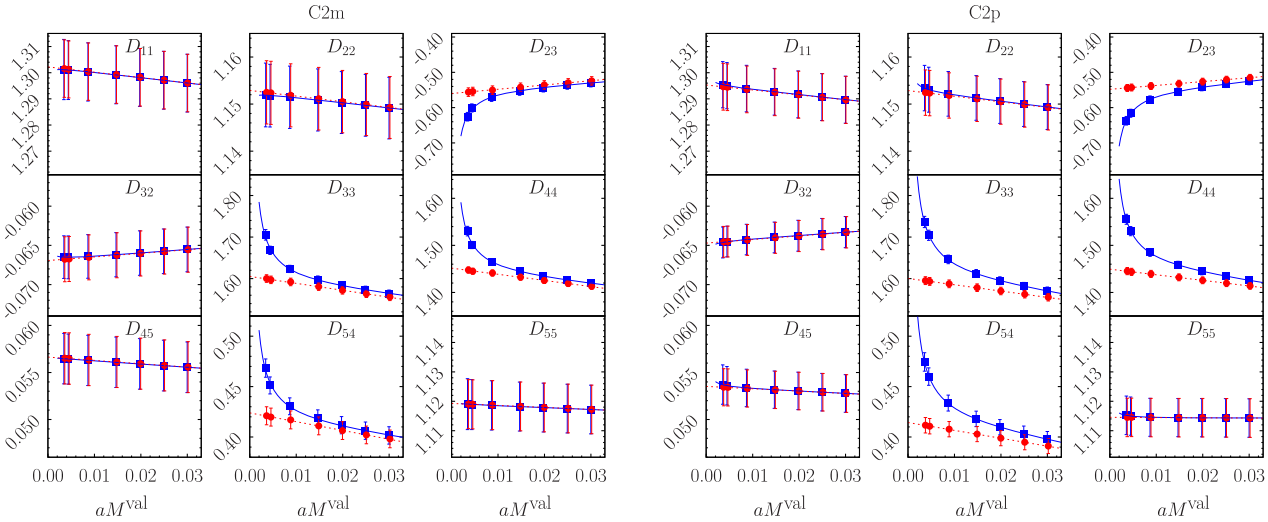

FIG. 15 (color online). Same as in Fig. 13 at $\beta = 2.10$, for the ensembles C2m (left) and C2p (right) and $(ap)^2 \simeq 1.57$.

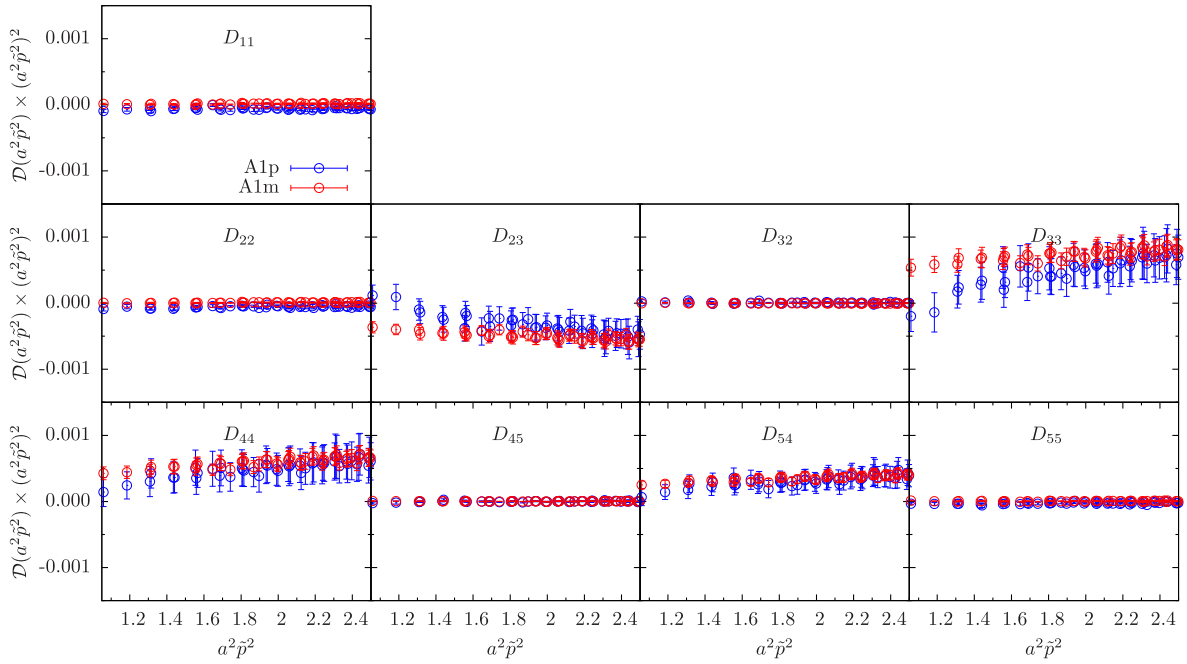

FIG. 16 (color online). For each of block-diagonal matrix element we form the product of $(a^2\tilde{p}^2)^2$ with the fit parameter $\mathcal{D}(a^2\tilde{p}^2)$ that is associated to the term of the double GB pole [cf. Eq. (B5)] and we plot it against $(a^2\tilde{p}^2)$ for the ensembles A1p and A1m of $\beta = 1.90$.

extract our RC estimates. This finding also serves as a confirmation of the good fit quality in analyzing the double GB pole term. Second, we find that the double GB pole contribution is negligible for the case of D_{11}, in nice agreement with theoretical expectations (see Ref. [62]), whereas it is different from zero for several of the D_{ij} with $i, j > 1$. So in our final analysis we have adopted single GB pole subtraction [i.e., set $\mathcal{D} = 0$ in the fit *Ansatz* of Eq. (B5)] for the former, single and double GB pole subtraction [cf. Eq. (B5)] for the latter cases.

(iii) After applying the θ-average of the RC estimators at each β and at each value of momentum defined by Eqs (A6) and (A7), which is required in order to achieve O(a)-improvement, we carry out the sea chiral limit for each element of the 5×5 renormalization matrix. A simple polynomial (linear) fit *Ansatz* fits the data smoothly. In Fig. 17 we illustrate an example of the chiral extrapolation

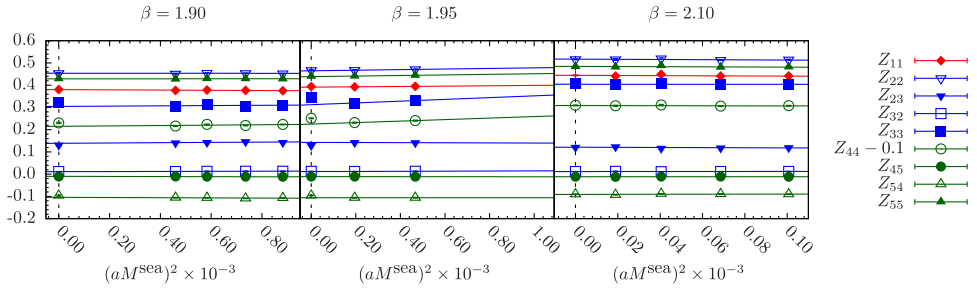

FIG. 17 (color online). Example of the sea chiral extrapolation of the RC estimators at three values of β computed at $(a\tilde{p})^2 \simeq 1.57$.

in the sea using almost the same value of momentum at the three β's.

(iv) Having performed the chiral limit extrapolations our estimates for the RCs take the form $Z_{ij}^{\rm RI'}(\tilde{p}^2;(a\tilde{p})^2) \equiv Z_{ij}^{\rm RI'}(\tilde{p}^2;(a\tilde{p})^2, aM^{\rm sea,val} = 0)$, where the first argument refers to the scale. Moreover we obtain the scale-independent off-diagonal elements, namely, $\Delta_{ij}^{\rm RI'}((a\tilde{p})^2) \equiv \Delta_{ij}^{\rm RI'}((a\tilde{p})^2, aM^{\rm sea,val} = 0)$. The estimators $Z_{ij}^{\rm RI'}(\tilde{p}^2;(a\tilde{p})^2)$ can be evolved to a common scale p_0 using the running formula for the operators Q_i known up to NLO [31,77], obtaining thus estimates of the form $Z_{ij}^{\rm RI'}(p_0^2;(a\tilde{p})^2)$. To be able to carry out a controlled study of the systematic discretization errors on the renormalized bag parameters, we apply the two methods proposed in Ref. [73]. We recall that each of these two methods, called M1 and M2, prescribes a different treatment of the cutoff effects. Method M1 consists of fitting $Z_{ij}^{\rm RI'}(p_0^2;(a\tilde{p})^2)$ to the linear *Ansatz*

$$Z_{ij}^{\rm RI'}(p_0^2;(a\tilde{p})^2) = Z_{ij}^{\rm RI'}(p_0^2) + \lambda_{ij} \times (a\tilde{p})^2 \quad \text{(B6)}$$

in some large momentum region. For better controlling the systematics we have made two choices, namely, $(a\tilde{p})^2 \in [1.5, 2.2]$ and $(a\tilde{p})^2 \in [1.8, 2.2]$.

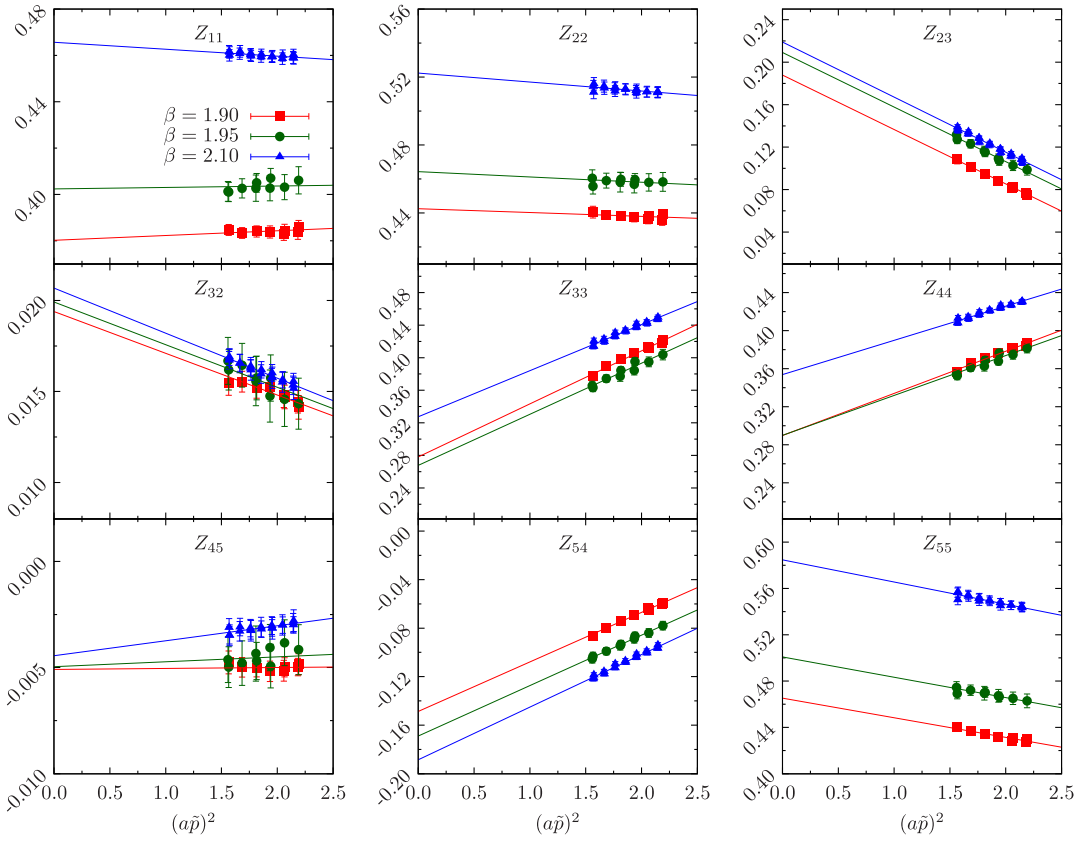

FIG. 18 (color online). Best linear fits [cf. Eq. (B6)] in the momentum interval $(a\tilde{p})^2 \in [1.8:2.2]$ for the block-diagonal RCs, Z_{ij}, at each value of β, renormalized in the $\overline{\rm MS}$ scheme at the scale of 3 GeV.

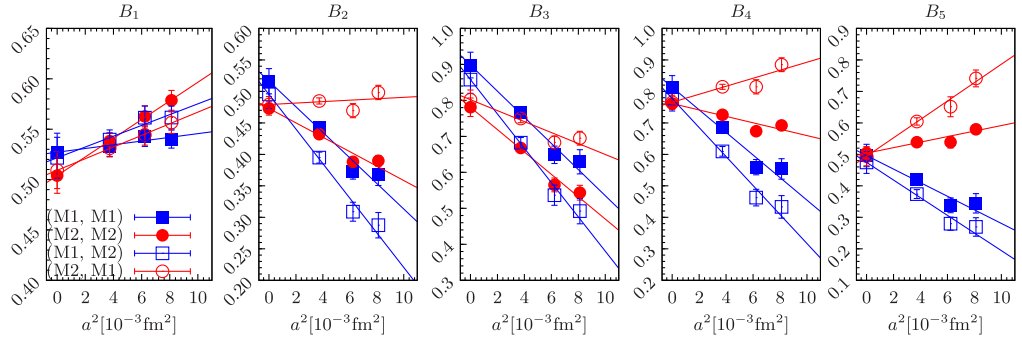

FIG. 19 (color online). $B_{1,\ldots,5}$ estimates computed at the physical strange quark value and at a fixed reference quark mass $\mu_\ell^{\mathrm{ref}} = 12.0$ MeV plotted against a^2 for the three values of the lattice spacing. We compare the scaling behavior of the bag-parameter estimates computed with the four possible combinations of M1 and M2 type for the four- and two-fermion RCs. The best linear fit in a^2 and the corresponding C.L. value for each RC combination is also shown.

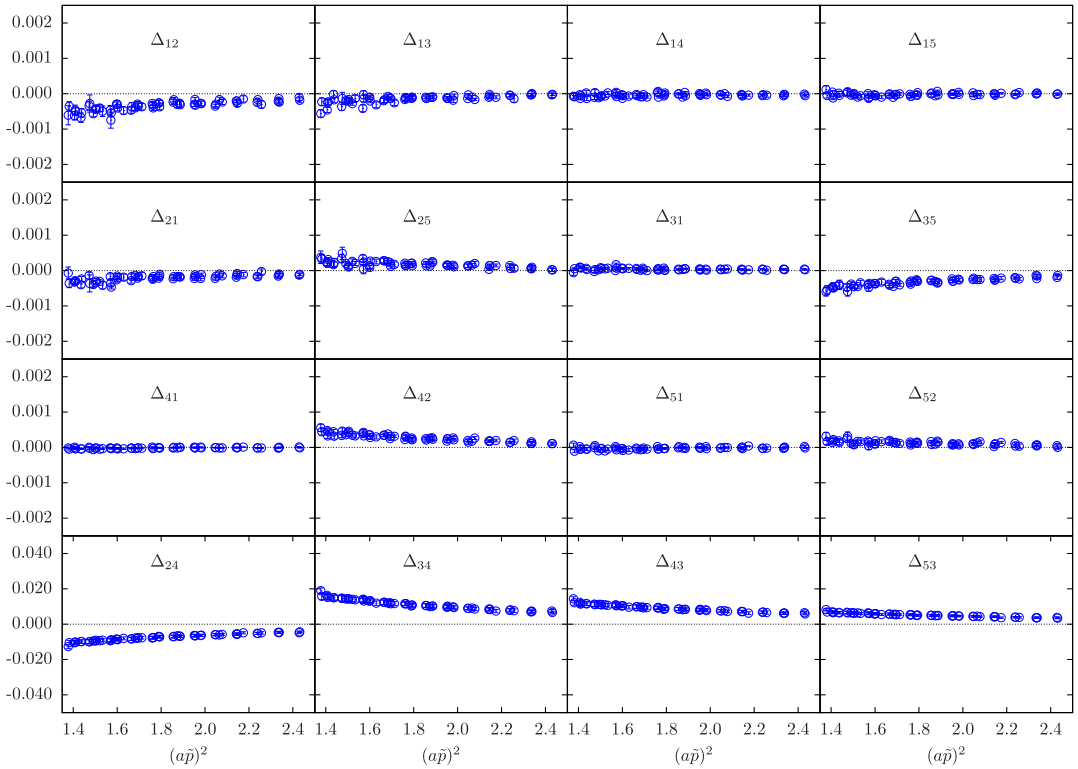

FIG. 20 (color online). The behavior of the off-diagonal mixing coefficients Δ_{ij} as a function of $(a\tilde{p})^2$ for $\beta = 2.10$.

As expected, thanks to subtraction of the perturbative $\mathrm{O}(a^2g^2)$ effects, the slopes λ_{ij} show very smooth dependence on β. In fact we parametrize the slopes in Eq. (B6) as $\lambda_{ij} = \lambda_{ij}^{(0)} + \lambda_{ij}^{(1)} g^2$ and we perform a simultaneous linear extrapolation to $(a\tilde{p})^2 = 0$ at all values of β. Then we may convert the extrapolated results $Z_{ij}^{\mathrm{RI}'}(p_0)$ to any scale and scheme as for example the $\overline{\mathrm{MS}}$ scheme using NLO running. In Fig. 18 we show the best linear fits of Z_{ij} (in the $\overline{\mathrm{MS}}$ scheme at the scale of 3 GeV) using Eq. (B6). The M2 method works in a quite different way from M1. It consists of getting the average RC value in a narrow window of momenta which is fixed in physical units for all values of β. We have carried out the M2-type analysis for two choices of momentum interval, namely, $\tilde{p}^2 \in [10\!:\!13]$ GeV^2 and $\tilde{p}^2 \in [11\!:\!14]$ GeV^2. These rather high values of momentum offer the possibility to gain more confidence in the absence of hadronic state contaminations and in the validity of the RC evolution using the NLO anomalous dimension at the price,

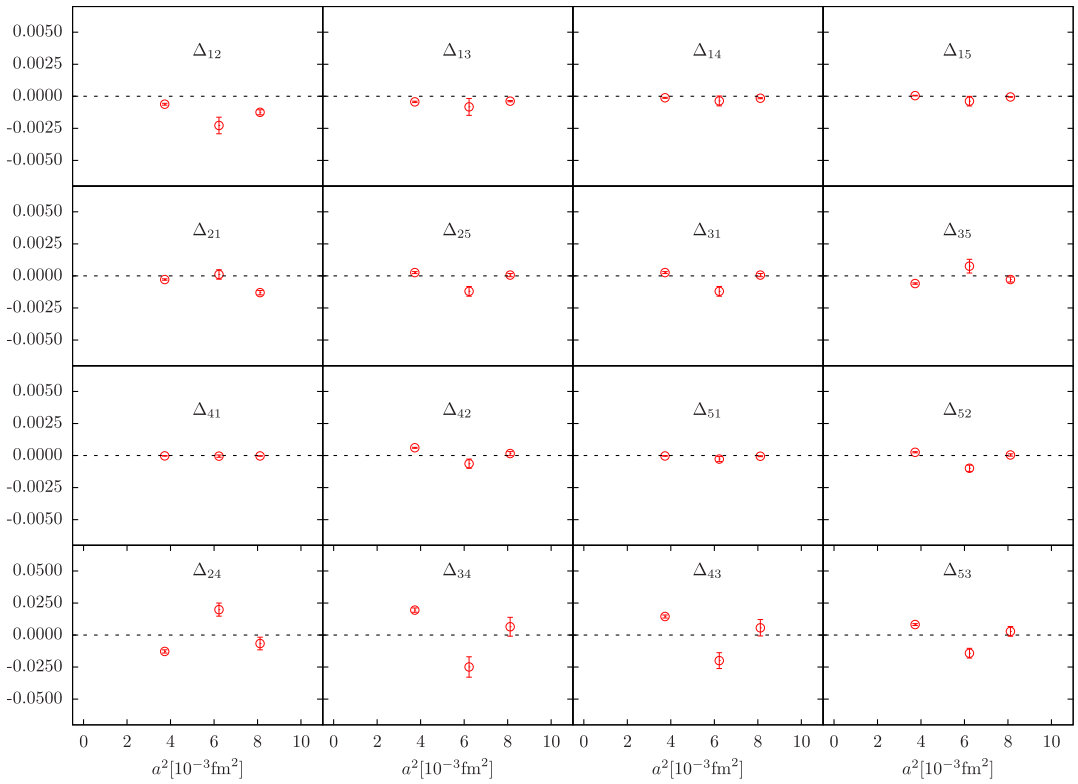

FIG. 21 (color online). Δ_{ij} computed with the M2 method against a^2.

however, of taking no special care to end up with reduced $O(a^2)$ cutoff effects.

In order to get an immediate view of the impact of the RC cutoff effects on the continuum limit estimates for the bag parameters, we have performed a scaling test for all B_i $(i = 1, \ldots, 5)$ which, for the case of the neutral K-mixing, is illustrated in Fig. 19. By using M1- or M2-type RCs we get the bag parameter estimates at some fixed reference value of the light quark mass and then we extrapolate them linearly in a^2 to the continuum limit. From the relevant panels of Fig. 19 it can be noticed that for both RC types[12] the a^2-scaling behavior is good and the extrapolated continuum limit results are compatible within 1 or 2 standard deviations, depending on the case.

The situation presented in Fig. 19 has to be considered as purely indicative but representative of the fact that at some arbitrary reference value of the light quark mass, using all four possible combinations of the RCs, the results for $B_{i=1,\ldots,5}$ converge to continuum limit values that are compatible within each other. We find this result very reassuring since M1- and M2-type RCs are computed in such a way that the corresponding cutoff effects are much different, though of $O(a^2)$. In this sense, by using two types of RCs we gain confidence that systematic effects due to the RC RI-MOM computation and discretization effects are under control. We also recall that for our final results we do not rely on plots like the ones presented in Fig. 19, but we perform combined chiral and continuum limit fits as those described by the fit *Ansätze* of Eqs. (2.13)–(2.15).

Finally, in Fig. 20 we depict the behavior of the scale-independent off-diagonal matrix elements Δ_{ij} for $\beta = 2.10$, while in Fig. 21 we plot the final estimates for Δ_{ij} against a^2. We note that in all cases Δ_{ij}'s get small values around zero. For the reader's convenience, we collect in the last row of Fig. 21 the Δ_{ij}'s for which we observe relatively larger values.

As we have anticipated in Sec. III, in order to take into account possible residual cutoff effects, in our final set of analyses we have included results for the bag parameters computed both with $\Delta_{ij} = 0$ and $\Delta_{ij} \neq 0$.

We collect for convenience the RCs for the bilinear quark operators, calculated in Ref. [65], in Table VII, while in Tables VIII and IX we summarize the RC values for the four-fermion operators.

[12]Notice that we have considered four cases corresponding to all possible combinations of taking M1- and M2-type RCs for the four- and two-fermion operators.

TABLE VII. Bilinear RCs published in Ref. [65]. The scale-independent Z_V, Z_A and the scale-dependent Z_P, Z_S, and Z_q are obtained with the methods M1 and M2. The scale-dependent RCs are expressed in the $\overline{\text{MS}}$ scheme at the scale of 3 GeV. Z_V is also obtained by performing a very accurate computation employing the Ward-Takahashi identity (WTI); for details see Sec. 2.3 of Ref. [73].

β	Method	Z_V	Z_A	Z_P	Z_S	Z_q
	M1	0.587(04)	0.731(08)	0.587(08)	0.830(14)	0.705(05)
1.90	M2	0.608(03)	0.703(02)	0.637(06)	0.974(04)	0.720(02)
	WTI	0.5920(04)				
	M1	0.603(03)	0.737(05)	0.566(05)	0.812(09)	0.719(04)
1.95	M2	0.614(02)	0.714(02)	0.606(03)	0.913(03)	0.727(01)
	WTI	0.6095(03)				
	M1	0.655(03)	0.762(04)	0.572(02)	0.777(06)	0.759(04)
2.10	M2	0.657(02)	0.752(02)	0.605(02)	0.832(04)	0.760(02)
	WTI	0.6531(02)				

TABLE VIII. Typical values for the four-fermion operator RCs at three values of β. For the M1 method, linear extrapolation to $(a\tilde{p})^2$ has been performed using data in the interval $(a\tilde{p})^2 \in [1.8, 2.2]$, while for method M2 we have used data from the narrow momentum window determined by $\tilde{p}^2 \in [11:14]$ GeV^2. RCs are expressed in the RI′ scheme at the scale of 3 GeV.

RI′ (3 GeV)	$\beta = 1.90$		$\beta = 1.95$		$\beta = 2.10$	
Z_{ij}	M1	M2	M1	M2	M1	M2
Z_{11}	0.373(07)	0.383(03)	0.395(05)	0.398(05)	0.454(04)	0.455(03)
Z_{22}	0.450(07)	0.450(04)	0.474(06)	0.469(05)	0.536(07)	0.528(04)
Z_{23}	0.200(07)	0.073(03)	0.222(05)	0.122(05)	0.236(03)	0.175(02)
Z_{32}	0.015(02)	0.009(01)	0.015(01)	0.010(01)	0.015(00)	0.013(00)
Z_{33}	0.247(11)	0.382(04)	0.237(07)	0.337(05)	0.285(06)	0.335(02)
Z_{44}	0.277(08)	0.368(03)	0.277(06)	0.344(04)	0.333(05)	0.362(02)
Z_{45}	−0.012(01)	−0.010(00)	−0.012(01)	−0.010(01)	−0.012(01)	−0.011(00)
Z_{54}	−0.146(05)	−0.054(02)	−0.166(04)	−0.090(03)	−0.187(03)	−0.141(02)
Z_{55}	0.435(07)	0.403(03)	0.471(05)	0.439(05)	0.552(07)	0.533(04)

TABLE IX. Same as in Table VIII, but in the $\overline{\text{MS}}$ scheme of [31] at the scale of 3 GeV.

$\overline{\text{MS}}$ (3 GeV)	$\beta = 1.90$		$\beta = 1.95$		$\beta = 2.10$	
Z_{ij}	M1	M2	M1	M2	M1	M2
Z_{11}	0.379(07)	0.389(03)	0.402(05)	0.404(06)	0.462(04)	0.462(03)
Z_{22}	0.440(07)	0.440(03)	0.463(06)	0.458(05)	0.524(07)	0.516(04)
Z_{23}	0.182(08)	0.050(03)	0.204(05)	0.101(05)	0.216(03)	0.153(02)
Z_{32}	0.020(02)	0.013(01)	0.020(02)	0.014(01)	0.021(01)	0.017(00)
Z_{33}	0.293(13)	0.453(04)	0.281(08)	0.399(06)	0.339(07)	0.398(03)
Z_{44}	0.304(09)	0.405(03)	0.303(07)	0.378(05)	0.364(06)	0.397(03)
Z_{45}	−0.006(01)	−0.004(00)	−0.006(01)	−0.004(01)	−0.005(01)	−0.003(00)
Z_{54}	−0.143(06)	−0.042(02)	−0.163(04)	−0.081(03)	−0.183(03)	−0.134(02)
Z_{55}	0.460(08)	0.426(04)	0.497(06)	0.464(06)	0.584(08)	0.564(05)

[1] S. Glashow, J. Iliopoulos, and L. Maiani, Weak interactions with lepton-hadron symmetry, Phys. Rev. D **2**, 1285 (1970).

[2] M. Gaillard and B. W. Lee, Rare decay modes of the K-mesons in gauge theories, Phys. Rev. D **10**, 897 (1974).

[3] H. Albrecht *et al.* (ARGUS Collaboration), Observation of B0—anti-B0 mixing, Phys. Lett. B **192**, 245 (1987).

[4] M. Bona *et al.* (UTfit Collaboration), Model-independent constraints on $\Delta F = 2$ operators and the scale of new physics, J. High Energy Phys. 03 (2008) 049.

[5] G. Isidori, Y. Nir, and G. Perez, Flavor physics constraints for physics beyond the Standard Model, Annu. Rev. Nucl. Part. Sci. **60**, 355 (2010).

[6] F. Mescia and J. Virto, Natural SUSY and kaon mixing in view of recent results from lattice QCD, Phys. Rev. D **86**, 095004 (2012).

[7] J. Charles, S. Descotes-Genon, Z. Ligeti, S. Monteil, M. Papucci, and K. Trabelsi (CKMfitter Collaboration), Future sensitivity to new physics in B_d, B_s, and K mixings, Phys. Rev. D **89**, 033016 (2014).

[8] A. J. Buras and J. Girrbach, Towards the identification of new physics through quark flavour violating processes, Rep. Prog. Phys. **77**, 086201 (2014).

[9] J. Kersten and L. Velasco-Sevilla, Flavour constraints on scenarios with two or three heavy squark generations, Eur. Phys. J. C **73**, 2405 (2013).

[10] J. Charles, O. Deschamps, S. Descotes-Genon, H. Lacker, A. Menzel *et al.* (CKMfitter Collaboration), Current status of the Standard Model CKM fit and constraints on $\Delta F = 2$ new physics, Phys. Rev. D **91**, 073007 (2015).

[11] A. Bevan, M. Bona, M. Ciuchini, D. Derkach, E. Franco *et al.* (UTfit Collaboration), Standard Model updates and new physics analysis with the Unitarity Triangle fit, arXiv:1411.7233. Updates and more information at http://www.utfit.org/UTfit/.

[12] V. Bertone *et al.* (ETM Collaboration), Kaon mixing beyond the SM from $N_f = 2$ tmQCD and model independent constraints from the UTA, J. High Energy Phys. 03 (2013) 089; 07 (2013) 143(E).

[13] B. Aubert *et al.* (*BABAR* Collaboration), Evidence for D^0-anti-D0 Mixing, Phys. Rev. Lett. **98**, 211802 (2007).

[14] M. Staric *et al.* (Belle Collaboration), Evidence for $D^0 - \bar{D}^0$ Mixing, Phys. Rev. Lett. **98**, 211803 (2007).

[15] R. Aaij *et al.* (LHCb Collaboration), Measurement of $D^0 - \bar{D}^0$ Mixing Parameters and Search for CP Violation Using $D^0 \to K^+\pi^-$ Decays, Phys. Rev. Lett. **111**, 251801 (2013).

[16] A. Bevan *et al.* (UTfit Collaboration), The UTfit collaboration average of D meson mixing data: Winter 2014, J. High Energy Phys. 03 (2014) 123.

[17] Y. Amhis *et al.* (Heavy Flavor Averaging Group Collaboration), Averages of B-hadron, C-hadron, and tau-lepton properties as of early 2012, arXiv:1207.1158.Updates at http://www.slac.stanford.edu/xorg/hfag/.

[18] G. Blaylock, A. Seiden, and Y. Nir, The role of CP violation in D0 anti-D0 mixing, Phys. Lett. B **355**, 555 (1995).

[19] A. A. Petrov, Charm mixing in the standard model and beyond, Int. J. Mod. Phys. A **21**, 5686 (2006).

[20] E. Golowich, J. Hewett, S. Pakvasa, and A. A. Petrov, Implications of $D^0 - \bar{D}^0$ mixing for new physics, Phys. Rev. D **76**, 095009 (2007).

[21] O. Gedalia, Y. Grossman, Y. Nir, and G. Perez, Lessons from recent measurements of D0—anti-D0 mixing, Phys. Rev. D **80**, 055024 (2009).

[22] M. Ciuchini, E. Franco, D. Guadagnoli, V. Lubicz, M. Pierini, V. Porretti, and L. Silvestrini, $D - \bar{D}$ mixing and new physics: General considerations and constraints on the MSSM, Phys. Lett. B **655**, 162 (2007).

[23] G. Beall, M. Bander, and A. Soni, Constraint on the Mass Scale of a Left-Right Symmetric Electroweak Theory from the K(L) K(S) Mass Difference, Phys. Rev. Lett. **48**, 848 (1982).

[24] F. Gabbiani, E. Gabrielli, A. Masiero, and L. Silvestrini, A complete analysis of FCNC and CP constraints in general SUSY extensions of the standard model, Nucl. Phys. **B477**, 321 (1996).

[25] F. Gabbiani and A. Masiero, FCNC in generalized supersymmetric theories, Nucl. Phys. **B322**, 235 (1989).

[26] E. Gabrielli, A. Masiero, and L. Silvestrini, Flavor changing neutral currents and CP violating processes in generalized supersymmetric theories, Phys. Lett. B **374**, 80 (1996).

[27] C. Allton, L. Conti, A. Donini, V. Gimenez, L. Giusti, G. Martinelli, M. Talevi, and A. Vladikas, B parameters for delta $S = 2$ supersymmetric operators, Phys. Lett. B **453**, 30 (1999).

[28] R. Baron, P. Boucaud, J. Carbonell, A. Deuzeman, V. Drach *et al.* (ETM Collaboration), Light hadrons from lattice QCD with light (u,d), strange and charm dynamical quarks, J. High Energy Phys. 06 (2010) 111.

[29] R. Baron *et al.* (ETM Collaboration), Computing K and D meson masses with $N_f = 2 + 1 + 1$ twisted mass lattice QCD, Comput. Phys. Commun. **182**, 299 (2011).

[30] G. Martinelli, C. Pittori, C. T. Sachrajda, M. Testa, and A. Vladikas, A general method for nonperturbative renormalization of lattice operators, Nucl. Phys. **B445**, 81 (1995).

[31] A. Buras, M. Misiak, and J. Urban, Two loop QCD anomalous dimensions of flavor changing four quark operators within and beyond the Standard Model, Nucl. Phys. **B586**, 397 (2000).

[32] S. Aoki, Y. Aoki, C. Bernard, T. Blum, G. Colangelo *et al.* (FLAG Collaboration), Review of lattice results concerning low-energy particle physics, Eur. Phys. J. C **74**, 2890 (2014).

[33] N. Carrasco, Neutral meson oscillations on the lattice, arXiv:1410.0161.

[34] S. Durr, Z. Fodor, C. Hoelbling, S. Katz, S. Krieg *et al.*, Precision computation of the kaon bag parameter, Phys. Lett. B **705**, 477 (2011).

[35] J. Laiho and R. S. Van de Water, *Proc. Sci.*, LATTICE2011 (2011) 293 [arXiv:1112.4861].

[36] R. Arthur *et al.* (RBC and UKQCD Collaborations), Domain wall QCD with near-physical pions, Phys. Rev. D **87**, 094514 (2013).

[37] T. Bae *et al.* (SWME Collaboration), Neutral kaon mixing from new physics: Matrix elements in $N_f = 2 + 1$ lattice QCD, Phys. Rev. D **88**, 071503 (2013).

[38] T. Blum *et al.* (RBC, UKQCD Collaborations), Domain wall QCD with physical quark masses, arXiv:1411.7017.

[39] T. Bae *et al.* (SWME Collaboration), Improved determination of B_K with staggered quarks, Phys. Rev. D **89**, 074504 (2014).

[40] Y.-C. Jang, H. Jeong, J. Kim, S. Kim, W. Lee *et al.*, Calculation of BSM kaon B-parameters using staggered quarks, *Proc. Sci.*, LATTICE2014 (2014) 370 [arXiv:1411.1501].

[41] P. Boyle, N. Garron, and R. Hudspith (RBC and UKQCD Collaborations), Neutral kaon mixing beyond the standard model with $n_f = 2 + 1$ chiral fermions, Phys. Rev. D **86**, 054028 (2012).

[42] A. Lytle, P. Boyle, N. Garron, R. Hudspith, and C. Sachrajda (RBC-UKQCD Collaboration), Kaon mixing beyond the Standard Model, *Proc. Sci.*, LATTICE2013 (2014) 400.

[43] N. Carrasco, M. Ciuchini, P. Dimopoulos, R. Frezzotti, V. Gimenez *et al.* (ETM Collaboration), $D^0 - \bar{D}^0$ mixing in the standard model and beyond from $N_f = 2$ twisted mass QCD, Phys. Rev. D **90**, 014502 (2014).

[44] A. J. Buras, J.-M. Gérard, and W. A. Bardeen, Large N approach to kaon decays and mixing 28 years later: $\Delta I = 1/2$ rule, $\hat{B}_K$ and ΔM_K, Eur. Phys. J. C **74**, 2871 (2014).

[45] W. A. Bardeen, A. Buras, and J. Gérard, The B parameter beyond the leading order of $1/n$ expansion, Phys. Lett. B **211**, 343 (1988).

[46] A. Donini, V. Gimenez, L. Giusti, and G. Martinelli, Renormalization group invariant matrix elements of $\Delta S = 2$ and $\Delta I = 3/2$ four fermion operators without quark masses, Phys. Lett. B **470**, 233 (1999).

[47] R. Babich, N. Garron, C. Hoelbling, J. Howard, L. Lellouch, and Claudio Rebbi, $K^0 - \bar{K}^0$ mixing beyond the standard model and CP-violating electroweak penguins in quenched QCD with exact chiral symmetry, Phys. Rev. D **74**, 073009 (2006).

[48] C. Chang, C. Bernard, C. Bouchard, A. El-Khadra, E. Freeland *et al.*, Update on a short-distance D^0-meson mixing calculation with $N_f = 2 + 1$ flavors, *Proc. Sci.*, LATTICE2014 (2014) 384 [arXiv:1411.6086].

[49] H.-W. Lin, S. Ohta, A. Soni, and N. Yamada, Charm as a domain wall fermion in quenched lattice QCD, Phys. Rev. D **74**, 114506 (2006).

[50] D. Becirevic, V. Gimenez, G. Martinelli, M. Papinutto, and J. Reyes, B parameters of the complete set of matrix elements of delta $B = 2$ operators from the lattice, J. High Energy Phys. 04 (2002) 025.

[51] N. Christ, T. Izubuchi, C. Sachrajda, A. Soni, and J. Yu (RBCUKQCD Collaborations), Long distance contribution to the $K_L - K_S$ mass difference, Phys. Rev. D **88**, 014508 (2013).

[52] Z. Bai, N. Christ, T. Izubuchi, C. Sachrajda, A. Soni, and J. Yu, $K_L - K_S$ Mass Difference from Lattice QCD, Phys. Rev. Lett. **113**, 112003 (2014).

[53] R. Frezzotti and G. C. Rossi, Chirally improving Wilson fermions. II: Four-quark operators, J. High Energy Phys. 10 (2004) 070.

[54] R. Frezzotti and G. C. Rossi, Chirally improving Wilson fermions. I: O(a) improvement, J. High Energy Phys. 08 (2004) 007.

[55] R. Frezzotti and G. C. Rossi, Twisted-mass lattice QCD with mass non-degenerate quarks, Nucl. Phys. B, Proc. Suppl. **128**, 193 (2004).

[56] P. Boucaud *et al.* (ETM Collaboration), Dynamical twisted mass fermions with light quarks, Phys. Lett. B **650**, 304 (2007).

[57] P. Boucaud *et al.* (ETM Collaboration), Dynamical twisted mass fermions with light quarks: Simulation and analysis details, Comput. Phys. Commun. **179**, 695 (2008).

[58] R. Baron *et al.* (ETM Collaboration), Light meson physics from maximally twisted mass lattice QCD, J. High Energy Phys. 08 (2010) 097.

[59] K. Osterwalder and E. Seiler, Gauge field theories on the lattice, Ann. Phys. (Amsterdam) **110**, 440 (1978).

[60] M. Bochicchio, L. Maiani, G. Martinelli, G. Rossi, and M. Testa, Chiral symmetry on the lattice with Wilson fermions, Nucl. Phys. **B262**, 331 (1985).

[61] P. Dimopoulos, H. Simma, and A. Vladikas, Quenched B (K)-parameter from Osterwalder-Seiler tmQCD quarks and mass-splitting discretization effects, J. High Energy Phys. 07 (2009) 007.

[62] M. Constantinou *et al.* (ETM Collaboration), B_K-parameter from $N_f = 2$ twisted mass lattice QCD, Phys. Rev. D **83**, 014505 (2011).

[63] N. Carrasco, M. Ciuchini, P. Dimopoulos, R. Frezzotti, V. Gimenez *et al.* (ETM Collaboration), B-physics from $N_f = 2$ tmQCD: The Standard Model and beyond, J. High Energy Phys. 03 (2014) 016.

[64] Y. Iwasaki, Renormalization group analysis of lattice theories and improved lattice action: Two-dimensional nonlinear O(N) sigma model, Nucl. Phys. **B258**, 141 (1985).

[65] N. Carrasco *et al.* (ETM Collaboration), Up, down, strange and charm quark masses with $N_f = 2 + 1 + 1$ twisted mass lattice QCD, Nucl. Phys. **B887**, 19 (2014).

[66] M. Foster and C. Michael (UKQCD Collaboration), Quark mass dependence of hadron masses from lattice QCD, Phys. Rev. D **59**, 074503 (1999).

[67] C. McNeile and C. Michael (UKQCD Collaboration), Decay width of light quark hybrid meson from the lattice, Phys. Rev. D **73**, 074506 (2006).

[68] S. Gusken, A study of smearing techniques for hadron correlation functions, Nucl. Phys. B, Proc. Suppl. **17**, 361 (1990).

[69] M. Albanese *et al.* (APE Collaboration), Glueball masses and string tension in lattice QCD, Phys. Lett. B **192**, 163 (1987).

[70] D. Becirevic and G. Villadoro, Remarks on the hadronic matrix elements relevant to the SUSY $K^0 - \bar{K}^0$ mixing amplitude, Phys. Rev. D **70**, 094036 (2004).

[71] D. Becirevic, S. Fajfer, and J. F. Kamenik, Chiral behavior of the $B^0_{d,s} - \bar{B}^0_{d,s}$ mixing amplitude in the standard model and beyond, J. High Energy Phys. 06 (2007) 003.

[72] D. Becirevic and F. Sanfilippo, Theoretical estimate of the $D^* \to D\pi$ decay rate, Phys. Lett. B **721**, 94 (2013).

[73] M. Constantinou *et al.* (ETM Collaboration), Non-perturbative renormalization of quark bilinear operators with $N_f = 2$ (tmQCD) Wilson fermions and the tree-level improved gauge action, J. High Energy Phys. 08 (2010) 068.

[74] M. Constantinou, V. Lubicz, H. Panagopoulos, and F. Stylianou, O(a^2) corrections to the one-loop propagator

and bilinears of clover fermions with Symanzik improved gluons, J. High Energy Phys. 10 (2009) 064.

[75] M. Constantinou, P. Dimopoulos, R. Frezzotti, V. Lubicz, H. Panagopoulos, A. Skouroupathis, and F. Stylianou, Perturbative renormalization factors and $O(a^2)$ corrections for lattice 4-fermion operators with improved fermion/gluon actions, Phys. Rev. D **83**, 074503 (2011).

[76] A. Donini, V. Gimenez, G. Martinelli, M. Talevi, and A. Vladikas, Nonperturbative renormalization of lattice four fermion operators without power subtractions, Eur. Phys. J. C **10**, 121 (1999).

[77] M. Ciuchini, E. Franco, V. Lubicz, G. Martinelli, I. Scimemi, and L. Silvestrini, Next-to-leading order QCD corrections to $\Delta F = 2$ effective Hamiltonians, Nucl. Phys. **B523**, 501 (1998).